Probing TeV scale origin of neutrino mass at future lepton colliders via neutral and doubly-charged scalars

P. S. Bhupal Dev,[1,*] Rabindra N. Mohapatra,[2,†] and Yongchao Zhang[1,‡]

[1]*Department of Physics and McDonnell Center for the Space Sciences, Washington University,
St. Louis, Missouri 63130, USA*
[2]*Maryland Center for Fundamental Physics, Department of Physics, University of Maryland,
College Park, Maryland 20742, USA*

We point out how future lepton colliders can provide unique insight into the scalar sector of TeV scale models for neutrino masses with local $B - L$ symmetry. Our specific focus is on the TeV scale left-right model, which naturally embeds this $B - L$ symmetry. In particular, we make a detailed study of the lepton collider implications of the neutral (H_3) and doubly-charged ($H^{\pm\pm}$) scalars from the right-handed triplet Higgs that is responsible for the spontaneous breaking of the $B - L$ symmetry and implementing the seesaw mechanism. Due to mixing with other scalars, the neutral scalar H_3 could acquire sizable flavor violating couplings to the charged leptons. Produced on-shell or off-shell at the planned $e^+ e^-$ colliders, it would induce distinct lepton flavor violating signals like $e^+ e^- \to \mu^\pm \tau^\mp (+H_3)$, with the couplings probed up to $\sim 10^{-4}$ for a wide range of neutral scalar mass, which is well beyond the reach of current searches for charged lepton flavor violation. The Yukawa couplings of the doubly-charged scalar $H^{\pm\pm}$ to the charged leptons might also be flavor violating, which is correlated to the heavy right-handed neutrino masses and mixings. With a combination of the pair, single and off-shell production of $H^{\pm\pm}$ like $e^+ e^- \to H^{++} H^{--}$, $H^{\pm\pm} e^\mp \mu^\mp$, $\mu^\pm \tau^\mp$, the Yukawa couplings can be probed up to 10^{-3} at future lepton colliders, which is allowed by current lepton flavor data in a large region of parameter space. For both the neutral and doubly-charged cases, the scalar masses could be probed up to the few-TeV range in the off-shell channel.

I. INTRODUCTION

Exploring the scale of new physics responsible for neutrino masses is one of the major topics under intense focus in particle physics today. If the scale is near the grand unification theory (GUT) scale (or much higher than the multi-TeV range), the only ways to explore this would be via rare decays of leptons and via proton decay in GUT models, providing only a limited window for their search. The situation however changes drastically if the new physics scale is around a few TeV, which is theoretically quite plausible, thus opening up many more possible experimental probes. In particular, explorations at the high-energy frontier using existing as well as planned future colliders primarily designed for other studies of beyond-the-Standard-Model (SM) physics become viable and effective for probing the neutrino mass physics. The lepton colliders are particularly well suited to study this question since they provide clean signals, not "muddied" by the QCD jet background from the SM and other unrelated new physics scenarios. It is therefore no surprise that the literature using lepton colliders for studying neutrino mass physics is already quite extensive; see e.g., Refs. [1–50] for a partial list and Refs. [51,52] for reviews.

In this paper, we add to this literature by exploring how the planned lepton colliders can provide unique insight into a specific class of TeV scale seesaw models [53–57] for neutrino masses based on the left-right symmetric model (LRSM) of weak interactions [58–60]. The LRSM, originally proposed as a well-motivated extension of SM for providing an alternative approach to parity violation in low-energy processes, has since emerged as a model for neutrino masses via the seesaw mechanism. In this note we focus particularly on the scalar sector of the LRSM where the parity symmetry has been broken at a high scale so that the low-energy theory does not contain the left triplet with $B - L = 2$. We call this LRSM (in contrast with the version where the discrete parity is broken at the TeV scale). This model contains two unique particles, which are not part of

the SM or many beyond-SM scenarios and are particularly suited for the lepton collider searches: one is a hadrophobic neutral scalar connected to spontaneous breaking of $B - L$ symmetry that goes into the seesaw mechanism (called H_3, following the convention in Ref. [61]) and another is the right-handed (RH) doubly-charged scalar partner of this (called H^{++}), that is part of the $SU(2)_R$ multiplet that contains H_3. The hadron collider implications of the hadrophobic scalar were discussed in previous papers [61–63] and we continue this exploration in this paper in the context of lepton colliders like the Circular Electron-Positron Collider (CEPC) [64], International Linear Collider (ILC) [65], Future Circular Collider (FCC-ee) [66] and Compact Linear Collider (CLIC) [67].

The reason these two scalars are particularly interesting for studying the origin of neutrino masses is that in the LRSM, the couplings (denoted by $f_{\alpha\beta}$) of the hadrophobic scalar and the doubly-charged scalar to leptons are the ones that are responsible for the seesaw masses of the RH neutrinos (RHNs) i.e., $M_{N,\alpha\beta} = 2f_{\alpha\beta}v_R$. For a $B - L$ breaking scale v_R in the 5–8 TeV range so that the W_R is accessible at the LHC [68–75], the magnitudes of $f_{\alpha\beta}$ responsible to fit the neutrino oscillation data [76], i.e., the mass square differences and the mixing angles, are sizable and hence accessible at the lepton colliders, unless all the entries of the Dirac mass matrix m_D in the seesaw formula $m_\nu \simeq -m_D M_N^{-1} m_D^T$ are very tiny. There are of course constraints on some subsets of these couplings from rare lepton decays but they leave enough room for some of them being of order one. Furthermore, rare lepton decays generally probe products of two different f couplings whereas the lepton collider probes them individually [47]. A question one can of course ask is: do we really know that all the m_D entries in the seesaw formula are not very tiny making the f's similarly tiny and inaccessible? Two reasons to think that this may not be the case are that

   (i) there are interesting seesaw textures for neutrino masses where some of the m_D elements are sizable [77–84] for the TeV scale seesaw; and

   (ii) if we make the f couplings very small, the Yukawa couplings that go into m_D become very small and give a feeling of being unnatural in the sense that we just as well could have had Dirac neutrinos of sub-eV mass with Yukawa couplings $\lesssim 10^{-12}$ without requiring any seesaw in the first place.

Add to this the possibility that sizable Dirac mass terms can be measured in colliders by measuring the heavy-light neutrino mixing parameters $V_{\nu N}$ in the process $pp \rightarrow \ell^\pm \ell^\pm jj$ [72,85]. Finally, it is not just that left-right models provide a venue for such sizable f couplings but also that there can be other models (e.g., models with global $B - L$ [86]) with similar properties, making the probes of sizable f of great theoretical as well as experimental interest. Also, there exist well-motivated f matrix textures within the context of LRSM fully consistent with current neutrino

mass and other observations e.g., rare lepton decays [83]. We show in this paper the interesting range of f values that can be measured in the planned lepton colliders such as CEPC and ILC and can provide new ways to test these models. They will in any case provide complementary information to rare lepton decay constraints on the f couplings and make such studies interesting from the synergistic viewpoint of energy and intensity frontiers.

This paper is organized as follows. In Sec. II, we describe the essentials of the LRSM relevant for our discussion. We then focus in Sec. III on the production of the neutral scalar H_3 in future lepton colliders like CEPC and ILC, given its couplings to the other scalars, the heavy RHNs and the heavy W_R and Z_R bosons, as well as other relevant couplings. Special attention is paid to the production of lepton flavor violating (LFV) signals induced by the neutral scalar H_3, as an explicit example of the general proposal in Ref. [47]. Prospects in all the possible on-shell and off-shell production channels of H_3 are given in this section, some of which are well below the current low-energy LFV constraints [76]. The lepton collider physics for the RH doubly-charged scalar follows in Sec. IV, where all the flavor and collider constraints are summarized, and all the possible pair production, single production and off-shell production modes of the doubly-charged scalar are discussed, with potential LFV signals. As far as we know, this is the first complete list of the production of RH doubly-charged scalars at lepton colliders in the literature, with all the possible accompanying LFV signals taken into consideration, though some of the channels (and some of the flavor combinations) have been separately investigated before. Three particular textures of the $f_{\alpha\beta}$ matrix are also exemplified for the doubly-charged scalar in this section, as seen in Table V. We will summarize the main results and conclude in Sec. V.

II. SEESAW SCALARS IN THE LEFT-RIGHT MODEL

The LRSM is based on the gauge group $\mathcal{G}_{LR} \equiv SU(3)_C \times SU(2)_L \times SU(2)_R \times U(1)_{B-L}$ [58–60]. The quarks Q and leptons ψ are assigned to the following irreducible representations of $\mathcal{G}_{LR}$:

$$Q_{L,\alpha} = \begin{pmatrix} u_L \\ d_L \end{pmatrix}_\alpha : \left(\mathbf{3}, \mathbf{2}, \mathbf{1}, \frac{1}{3}\right),$$

$$Q_{R,\alpha} = \begin{pmatrix} u_R \\ d_R \end{pmatrix}_\alpha : \left(\mathbf{3}, \mathbf{1}, \mathbf{2}, \frac{1}{3}\right),$$

$$\psi_{L,\alpha} = \begin{pmatrix} \nu_L \\ e_L \end{pmatrix}_\alpha : (\mathbf{1}, \mathbf{2}, \mathbf{1}, -1),$$

$$\psi_{R,\alpha} = \begin{pmatrix} N_R \\ e_R \end{pmatrix}_\alpha : (\mathbf{1}, \mathbf{1}, \mathbf{2}, -1), \quad (1)$$

where $\alpha = 1, 2, 3$ represents the family indices, and the subscripts L, R denote the left and right chiral projection operators $P_{L,R} = (1 \mp \gamma_5)/2$, respectively.

In the LRSM, in addition to a bidoublet Higgs field $\Phi(2, 2, 0)$, a RH triplet Higgs field is introduced:

$$\Delta_R = \begin{pmatrix} \Delta_R^+/\sqrt{2} & \Delta_R^{++} \\ \Delta_R^0 & -\Delta_R^+/\sqrt{2} \end{pmatrix} : (\mathbf{1}, \mathbf{1}, \mathbf{3}, 2), \qquad (2)$$

in order to break the $SU(2)_R \times U(1)_{B-L}$ symmetry down to $U(1)_Y$ and to give mass to the heavy RHNs from the following Yukawa coupling:

$$\mathcal{L}_Y \supset f_{\alpha\beta} \psi_{R,\alpha}^T C^{-1} \sigma_2 \Delta_R \psi_{R,\beta} + \text{H.c.}, \qquad (3)$$

where C is the charge conjugation matrix, σ_2 is the second Pauli matrix, and $f_{\alpha\beta}$ are the Yukawa coupling matrix elements with α, β the lepton flavor indices. The singly-charged member of this triplet gets absorbed as the longitudinal mode of the heavy W_R boson and the imaginary part of the neutral component $\text{Im}\Delta_R^0$ as the longitudinal mode of the Z_R boson, leaving $H_3 \equiv \text{Re}(\Delta^0)$ and $H^{\pm\pm} \equiv \Delta_R^{\pm\pm}$ as physical fields. Note that the RHN mass matrix that goes into the seesaw formula is now determined by the vacuum expectation value (VEV) $\langle \Delta_R^0 \rangle = v_R$, viz. $M_{N,\alpha\beta} = 2 f_{\alpha\beta} v_R$. Therefore measuring the couplings of $H^{\pm\pm}$ is tantamount to measuring the RHN mass matrix. We show below how the planned lepton colliders like CEPC and ILC can probe deeper into the ranges of $f_{\alpha\beta}$, providing tests of certain LRSM-based neutrino mass models. We call H_3 and $H^{\pm\pm}$ the "seesaw Higgs bosons" due to their role in implementing the seesaw mechanism. For a detailed discussion of the symmetry breaking scalar sector of the LRSM, see e.g., Refs. [61,87–89].

III. THE NEUTRAL SCALAR

A unique property of the $SU(2)_R$ symmetry breaking neutral scalar H_3 in the LRSM is that it directly couples only to the heavy doubly-charged scalar $H^{\pm\pm}$ from the RH triplet Δ_R and the heavy scalars from the bidoublet Φ; the heavy gauge bosons W_R, Z_R; and the heavy RHNs N_α, but does not interact directly with the SM quarks; i.e., it is naturally a hadrophobic scalar [61]. Following Ref. [61], the interaction Lagrangian involving H_3 is given by

$$\begin{aligned} \mathcal{L}_{H_3} = {} & \frac{1}{2\sqrt{2}} \alpha_1 v_R H_3 hh - \frac{1}{\sqrt{2}} \alpha_1 v_{\text{EW}} h H_3 H_3 + 2\sqrt{2}(\rho_1 + 2\rho_2) v_R H_3 H^{++} H^{--} \\ & + \left(\frac{1}{\sqrt{2}} [\hat{Y}_U \sin\tilde{\theta}_1 - (V_L \hat{Y}_D V_R^\dagger) \sin\tilde{\theta}_2]_{\alpha\beta} H_3 \bar{u}_\alpha u_\beta + \frac{1}{\sqrt{2}} [\hat{Y}_D \sin\tilde{\theta}_1 - (V_L \hat{Y}_U V_R^\dagger) \sin\tilde{\theta}_2]_{\alpha\beta} H_3 \bar{d}_\alpha d_\beta \right. \\ & \left. + \frac{1}{\sqrt{2}} [\hat{Y}_E \sin\tilde{\theta}_1 - Y_{\nu N} \sin\tilde{\theta}_2]_{\alpha\beta} H_3 \bar{\ell}_\alpha \ell_\beta + f_{\alpha\beta} H_3 \overline{N_\alpha^C} N_\beta + \text{H.c.} \right) + \frac{c_{H_3\gamma\gamma}\alpha_{\text{EM}}}{4v_R} H_3 F_{\mu\nu} F^{\mu\nu} \\ & + \frac{1}{\sqrt{2}} g_L^2 \sin\theta_1 v_{\text{EW}} H_3 W_\mu^+ W^{-\mu} + \frac{g_L^2 \sin\theta_1 v_{\text{EW}}}{2\sqrt{2}\cos^2\theta_w} H_3 Z_\mu Z^\mu + \sqrt{2} g_R^2 v_R H_3 W_{R\mu}^+ W_R^{-\mu}, \end{aligned} \qquad (4)$$

In Eq. (4), v_{EW} is the electroweak VEV; $\hat{Y}_{U,D,E}$ are respectively the diagonal Yukawa couplings of the SM Higgs to the up-type quarks, down-type quarks and charged leptons; $V_{L,R}$ are the left- and right-handed quark mixing matrices; $Y_{\nu N} = m_D/v_{\text{EW}}$; $\sin\tilde{\theta}_{1,2} \equiv \sin\theta_{1,2} + \xi\sin\theta_{2,1}$ with $\xi = \kappa'/\kappa$ the ratio of the VEVs from the bidoublet Φ; α_1, ρ_1 and ρ_2 are respectively the coefficients for the quartic coupling terms $\text{TR}(\Phi^\dagger\Phi)\text{TR}(\Delta\Delta^\dagger)$, $[\text{TR}(\Phi^\dagger\Phi)]^2$ and $\text{TR}(\Delta\Delta)\text{TR}(\Delta^\dagger\Delta^\dagger)$ in the scalar potential; g_L is the gauge coupling for the $SU(2)_L$ gauge group; θ_w is the weak mixing angle; α and β are the quark/lepton flavor indices.

At the tree level, the scalar mass $m_{H_3}^2 = 4\rho_1 v_R^2$. For sufficiently small coupling ρ_1, the scalar mass m_{H_3} could be much smaller than the RH scale v_R. Then in this case the radiative corrections to m_{H_3} become important, and might even dominate the H_3 mass. However, using the Coleman-Weinberg effective potential [90], it was found that [62,63] the bosonic contributions to the H_3 mass from the heavy scalars and the heavy gauge bosons are partially canceled by those from fermionic heavy RHNs, which allows for H_3 masses much lighter than the v_R scale.[1] Here we treat m_{H_3} as a free parameter in an effective theory approach.

The couplings of H_3 to the heavy W_R boson and the singly and doubly-charged scalars induce an effective one-loop coupling of H_3 to two photons, as shown in Eq. (4), with α_{EM} the fine-structure constant and $c_{H_3\gamma\gamma}$ depending on the scalar and vector loop functions as a function of the mass m_{H_3} [62,63]. Note that this coupling is effectively suppressed by the RH scale v_R and in the limit of $m_{H_3} \ll v_R$, the coefficient $c_{H_3\gamma\gamma}$ approaches a numerical constant $\simeq 4\sqrt{2}/3\pi$.

---

[1]As long as the scalar, Yukawa and gauge couplings for the loop contribution to m_{H_3} are perturbative, the higher-loop contributions are expected to be smaller than the one-loop diagrams.

The H_3 could of course mix with the SM Higgs h as well as with the heavy CP-even scalar H_1 from the bidoublet Φ, due to the $\text{Tr}(\Phi^\dagger\Phi)\text{Tr}(\Delta_R\Delta_R^\dagger)$-type quartic interaction, with the corresponding mixing angles $\sin\theta_1$ and $\sin\theta_2$ respectively. This induces the (flavor-changing) couplings of H_3 to the SM fermions and to the W and Z bosons.[2] In some specific scenarios the heavy-light neutrino mixings might be sizable [83], and generate the couplings of H_3 to the light active neutrinos, depending also on the magnitude of the f couplings in Eq. (3).

The H_3 could mix with the heavy neutral component H_1 from the bidoublet Φ, thereby acquiring tree-level flavor-changing neutral current (FCNC) couplings in both the quark and lepton sectors [62,63]. In light of the seesaw mechanism, the flavor structure of the FCNC couplings of H_3 in the lepton sector is different from that in the quark sector. In particular, the flavor-changing couplings of H_3 to the charged leptons are dictated by the Dirac neutrino mass matrix m_D. In the most general cases, m_D is not diagonal, as it has to be used to generate the mixings of active neutrinos. Furthermore, in some circumstances some elements of $Y_{\nu N}$ might be sizable, even of order $\mathcal{O}(0.1)$ [83], which is essential to have large effective couplings of H_3 to the charged leptons. For a heavy H_3, the mixing angle with H_1 could even reach up to the order of 0.1 [62,63]; then it is possible to have an effective coupling $h_{\alpha\beta}$ of order 0.01 in some region of the parameter space. For the sake of concreteness and conciseness, we write the LFV couplings of H_3 in an effective form, without explicit dependence on the parameters in the charged lepton mass matrix, the Dirac neutrino mass matrix, or the RHN mass matrix:

$$\mathcal{L}_{H_3} \supset h_{\alpha\beta}H_3\bar\ell_\alpha\ell_{\beta,} + \text{H.c.}, \qquad (5)$$

with α, $\beta = e$, μ, τ. For simplicity we also assume the coupling matrix $h_{\alpha\beta}$ is real and symmetric [47].[3] The LFV couplings of H_3 to the charged leptons could also be induced radiatively through the doubly-charged loop,

which is however highly suppressed by the mass ratio $m_\ell^2/M_{\pm\pm}^2$ (m_ℓ and $M_{\pm\pm}$ being respectively the charged lepton and doubly-charged scalar mass) and the loop factor [93]. For the few TeV RH scale v_R, the loop-level decay is comparable to the tree-level width only when the effective coupling $h \sim 10^{-8}$ in Eq. (4), which is far below the future prospects (see Figs. 18 and 19); thus the loop-level LFV couplings of H_3 can be safely neglected in this paper. One should note that the Dirac neutrino mass matrix m_D, and consequently the effective coupling $h_{\alpha\beta}$ in Eq. (4), might also be tested by other future lepton data, e.g., the rare RHN decay $N \to W^\pm\ell^\mp$, the electron EDM, neutrinoless double beta decay and neutrino transition moments [94]. These experiments depend however also on the RHN masses and mixings, the CP violating phases in m_D, and/or even the $W - W_R$ mixing angle, and might be largely complementary to the direct searches of the "smoking-gun" beyond-SM LFV signals at future lepton colliders.

The couplings of H_3 collected in Eq. (4) lead to very rich phenomenology for the production and decay of H_3 in future lepton colliders like CEPC, ILC, FCC-ee and CLIC, even though some of the heavy particles cannot be directly produced on shell at these colliders. We first present the decay branching ratios (BR) of H_3, before moving on to its production modes.

A. H_3 decay branching ratios

For illustration purposes, two examples of decay BRs of the neutral scalar H_3 are shown in Fig. 1, with a sizable mixing with the SM Higgs, $\sin\theta_1 = 0.01$ (left), and without any mixing, $\sin\theta_1 = 0$ (right). The H_3 decays into the SM particles, like the W, Z, h bosons, quarks, charge leptons and gluons, only due to its mixing with h, and therefore, all of these partial decay widths are proportional to $\sin^2\theta_1$. The decay $H_3 \to \gamma\gamma$ receives two contributions: one from the SM top quark and W boson loops via mixing with the SM Higgs, and the other one from the heavy W_R boson and the heavy charged scalar loops which are suppressed by the v_R scale. For concreteness we have set $v_R = 5$ TeV in Fig. 1. For the LFV decays $H_3 \to \ell_\alpha^\pm\ell_\beta^\mp$, we adopt a benchmark value of $h = 10^{-2}$ for the effective LFV couplings [cf. Eq. (4)], which is still allowed by current lepton flavor data in a large parameter space for $m_{H_3} \gtrsim 10$ GeV (see Figs. 18 and 19 for more details). The analytic expressions for the partial decay widths of H_3 can be found in Refs. [62,63]. It is clear in the left panel of Fig. 1 that when the neutral scalar is light, i.e., $m_{H_3} \lesssim 2m_{W,Z}$, it decays predominantly into the LFV lepton pairs, as all the other channels are either suppressed by the small couplings in the SM (like the light quarks) or loop suppressed (like gluons and photons). When the decays $h_3 \to WW$, ZZ, hh are open, they will take over as the dominant channels, as they grow as $\Gamma(H_3 \to WW, ZZ, hh) \propto G_F m_{H_3}^3$ (G_F being the Fermi constant), much faster than the LFV channel.
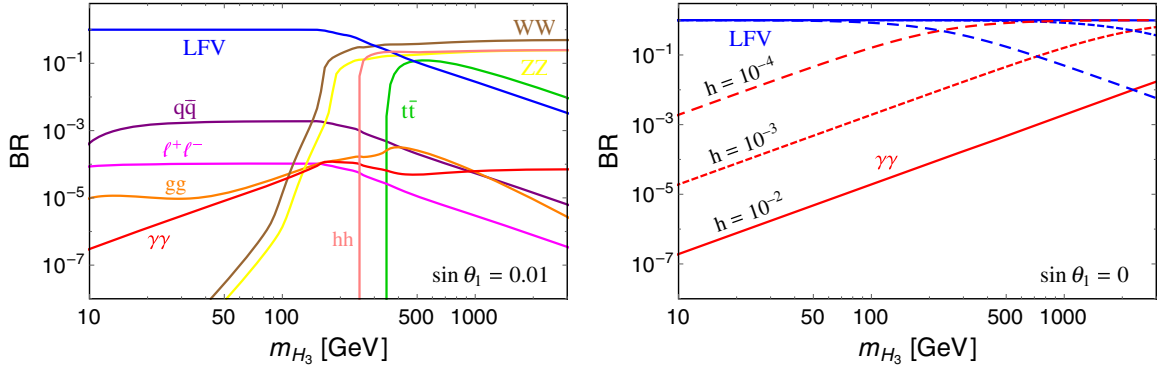
---

[2]The $W - W_R$ and $Z - Z_R$ mixings contribute also to the couplings of H_3 to the SM W and Z bosons, but they are heavily suppressed respectively by the mass ratios $\sim m_W^2/m_{W_R}^2$ and $m_Z^2/m_{Z_R}^2$ [61,88] and are neglected here.

[3]The symmetric properties of the leptonic Yukawa couplings and the Dirac matrix m_D depend on how the left- and right-handed leptons $\psi_{L,R}$ and the bidoublet Φ transform under the parity symmetry, but not on how parity is broken at the TeV or higher energy scale, e.g., whether the left-handed triplet decouples from the TeV scale physics, as the matrix m_D does not come from couplings to the triplets. These fields transform as $\Phi \leftrightarrow \Phi^\dagger$ and $\psi_L \leftrightarrow \psi_R$ under parity P, so the Yukawa coupling matrices for the leptons are required to be Hermitian [91]. There are of course small radiative corrections below the scale of the triplet mass but they are proportional to $y^2/16\pi^2$ (with y the Yukawa couplings) and are therefore very small, maintaining the symmetric property for all practical purposes. More discussion of generalized parity can be found in e.g., Ref. [92].

FIG. 1. Left: The decay BRs of the neutral scalar H_3 into the WW, ZZ bosons; the light quarks $q\bar{q}$ (with $q = u, d, s, c, b$); the top pair $t\bar{t}$; the charged leptons $\ell^+\ell^-$; the gluon pair gg; the photon pair $\gamma\gamma$; and the charged lepton pairs with the LFV signal (LFV). The mixing with the SM Higgs $\sin\theta_1 = 0.01$, the RH scale $v_R = 5$ TeV and the LFV coupling $h = 0.01$. For concreteness, the bidoublet VEV ratio $\xi = \kappa'/\kappa$ has been set to m_b/m_t as in Refs. [62,63], and the mixing angle $\sin\theta_2$ with the heavy scalar H_1 is set to be zero. Right: The decay BRs of H_3 into $\gamma\gamma$ (red) and LFV lepton pairs (blue) without mixing with the SM Higgs ($\sin\theta_1 = 0$) and $v_R = 5$ TeV, for three benchmark values of $h = 10^{-2}$ (solid line), 10^{-3} (short-dashed) and 10^{-4} (long-dashed).

In the limit of $\sin\theta_1 \to 0$, all the couplings of the SM Higgs approach to their SM values [61]. In this alignment limit, the neutral scalar could only decay into two photons induced from the heavy charged particles in the $SU(2)_R$ sector, and into the LFV charged leptons from mixing with the heavy scalar H_1. The fraction $\text{BR}(H_3 \to \ell_\alpha \ell_\beta) = 1 - \text{BR}(H_3 \to \gamma\gamma)$ depends largely on the v_R scale and the effective LFV coupling h [cf. Eq. (4)]. Given v_R fixed at 5 TeV, three benchmark values of $h = 10^{-2}$, 10^{-3} and 10^{-4} are shown in the right panel of Fig. 1, depicted respectively as solid, short-dashed and long-dashed contours. As seen in this plot, for the LFV coupling $h \gtrsim 10^{-3}$, the BR of the diphoton channel is very small for $m_{H_3} \lesssim$ TeV, as it is suppressed both by the loop factors and by the v_R scale. As $\Gamma(H_3 \to \gamma\gamma) \propto m_{H_3}^3/v_R^2$ and $\Gamma(H_3 \to \ell\ell) \propto m_{H_3}$, the diphoton width grows much faster than the dilepton channel when m_{H_3} gets heavier and becomes important for $h \sim 10^{-4}$ and $m_{H_3} \gtrsim$ few hundred GeV.

B. Production of H_3

Based on the scalar, Yukawa and gauge interactions in Eq. (4), the production of H_3 at an e^+e^- collider can be categorized into five groups:

(i) *Doubly-charged scalar portal:* Through the fusion of the doubly-charged scalar pair, $H^{+++*}H^{--*} \to H_3$ with the trilinear scalar interaction $H_3 H^{++} H^{--}$ related to their masses [61]. The virtual doubly-charged scalars are emitted from the initial electron/positron via the Yukawa interaction $f_{\alpha\beta}$, inducing potentially the LFV signal if $\alpha \neq \beta$; see Fig. 2.

(ii) *Gauge portal:* Through the effective one-loop coupling to diphoton $\gamma\gamma \to H_3$, with subleading contribution from $e^+e^- \to \gamma^* \to \gamma H_3$ and $\gamma^*\gamma^* \to H_3$; see Fig. 4.

(iii) *SM Higgs portal:* Through mixing with SM Higgs $e^+e^- \to Z^* \to ZH_3$ (and other subleading production modes like through the fusion of SM W and Z bosons); see Fig. 6.

(iv) *Neutrino portal:* Through the fusion of (heavy) RHNs, which couples to the initial electron/positron via the heavy-light neutrino mixing $N_\alpha^* N_\beta^* \to H_3$; see Fig. 8.

(v) *Heavy scalar portal:* The LFV couplings of H_3 [cf. Eq. (4)] will induce various production modes, like the on-shell production $e^+e^- \to (\gamma/Z)H_3$ and $e^+e^- \to (\ell_\alpha^+\ell_\beta^-/\nu_\alpha\bar{\nu}_\beta)H_3$ and the H_3-mediated processes $e^+e^- \to \ell_\alpha^+\ell_\beta^-$ [47]. See Figs. 9, 11, 13 and 15.

We discuss below each of these production modes in some details. To be specific, we focus in this paper only on the CEPC and ILC as two benchmark machines for future lepton colliders. However, for comparison, we present in Table I the planned final center-of-mass energy $\sqrt{s}$, the expected integrated luminosity and the required running time to achieve this luminosity for the four lepton colliders under discussion, viz. CEPC, ILC, FCC-ee and CLIC [95]. The center-of-mass energies and luminosities at FCC-ee
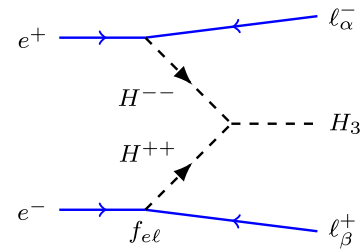

FIG. 2. Feynman diagram for the production of H_3 at lepton colliders from the doubly-charged scalar fusion.

TABLE I. The planned final center-of-mass energy $\sqrt{s}$, the expected integrated luminosity and the required running time to achieve this luminosity for the four future lepton colliders [95].

Collider	$\sqrt{s}$ (GeV)	Luminosity (ab^{-1})	Running time (years)
CEPC	240	5	7
FCC-ee	250	5	3
ILC	1000	1	8–10
CLIC	3000	3	6–8

and CLIC are expected to be comparable or higher than those at CEPC and ILC and could therefore improve to some extent the prospects at CEPC and ILC discussed in this paper. In this sense, the results in this paper can be considered to be conservative, at least in some of the channels.

C. Doubly-charged scalar portal

For the coupling of H_3 to the doubly-charged scalar $H^{\pm\pm}$ in Eq. (4),

$$(\rho_1 + 2\rho_2)v_R = \frac{m_{H_3}^2}{4v_R} + \frac{M_{\pm\pm}^2}{2v_R}, \qquad (6)$$

where we have used the fact that the neutral and doubly-charged scalar masses are respectively $m_{H_3}^2 = 4\rho_1 v_R^2$ and $M_{\pm\pm}^2 = 4\rho_2 v_R^2$ [61]. In the limit of $m_{H_3} \ll v_R$ and $M_{\pm\pm} \gg \sqrt{s}$, the dependence of the trilinear scalar coupling on the doubly-charged scalar mass cancels partially the suppression of the heavy $H^{\pm\pm}$ propagator $(1/M_{\pm\pm}^2)^2$ in Fig. 2, leaving only a $\sim 1/M_{\pm\pm}^2$ dependence on the doubly-charged scalar mass. The couplings of $H^{\pm\pm}$ to the SM charged leptons stem from the $f_{\alpha\beta}$ term in Eq. (3) and might be flavor changing, i.e.,

$$e^+ e^- \to \ell_\alpha^+ \ell_\beta^- H_3 \qquad (7)$$

with $\alpha, \beta \neq e$. In light of the clean environment at lepton colliders, this would definitely point to new physics beyond the SM. The production cross section contours at $\sqrt{s} = 1$ TeV are shown in Fig. 3, as functions of the doubly-charged scalar mass $M_{\pm\pm}$ and $|f_{ee}|$, for the benchmark values of $v_R = 5$ TeV and in the limit of small m_{H_3}. The initial state radiation (ISR) and beamstrahlung have been taken into consideration for the colliding beams and $p_T > 10$ GeV imposed for the $e^\pm$ in the final state, implemented by using CalcHEP [96]. We have assumed that the initial beams are polarized, i.e., $P_{e^-} = 0.8$ and $P_{e^+} = -0.3$, which enhance the couplings to the RH doubly-charged scalar by a factor of $(1 + P_{e^-})(1 - P_{e^+}) = 2.34$ compared to the unpolarized beams. Limited by a smaller $\sqrt{s} = 240$ GeV, the cross sections at CEPC are expected to be much smaller.
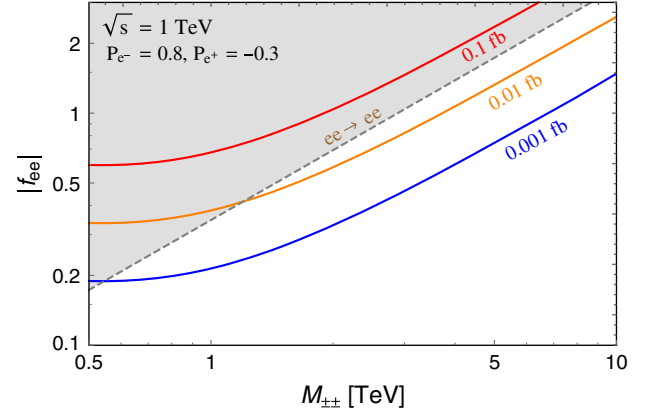

FIG. 3. Production cross section contours of H_3 at ILC 1 TeV with polarized beams ($P_{e^-} = 0.8$, $P_{e^+} = -0.3$) through the doubly-charged scalar fusion in the channel $e^+ e^- \to e^+ e^- H_3$ (see Fig. 2), as functions of $M_{\pm\pm}$ and $|f_{ee}|$, in the limit of $m_{H_3} \ll M_{\pm\pm}$. The shaded region is excluded by the LEP $ee \to ee$ data [97]. See text for more details.

In the limit of small mixing with other scalar particles, the neutral scalar H_3 decays predominantly into two photons $H_3 \to \gamma\gamma$ through the W_R and charged scalar loops, or into a pair of charged leptons, as detailed in Sec. III G with the signal of $e^+ e^- \to \ell_\alpha \ell_\beta (H_3 \to \gamma\gamma, \ell_\gamma \ell_\delta)$.

With the lepton flavor conserving and violating couplings $f_{\alpha\beta}$, the doubly-charged scalar contributes to the electron and muon $g - 2$, rare charged lepton decays $\ell_\alpha \to \ell_\beta \gamma$, $\ell_\alpha \to \ell_\beta \ell_\gamma \ell_\delta$, muonium-antimuonium oscillation and $ee \to \ell\ell$. All the flavor limits on the Yukawa couplings are collected in Table IV in Sec. IV A. The LFV signals $\ell_\alpha \ell_\beta = e\mu$, $e\tau$ and $\mu\tau$ in Eq. (7) depend on the combinations of Yukawa couplings $|f_{ee}^\dagger f_{e\mu}|$, $|f_{ee}^\dagger f_{e\tau}|$ and $|f_{e\mu}^\dagger f_{e\tau}|$, which are tightly constrained respectively by the rare decays $\mu \to eee$, $\tau \to eee$ and $\tau^- \to \mu^- e^+ e^-$. For instance, for $M_{\pm\pm} = 500$ GeV, the limits are respectively

$$|f_{ee}^\dagger f_{e\mu}|^2 < 3.3 \times 10^{-11},$$
$$|f_{ee}^\dagger f_{e\tau}|^2 < 5.2 \times 10^{-6},$$
$$|f_{e\mu}^\dagger f_{e\tau}|^2 < 2.6 \times 10^{-6}, \qquad (8)$$

which make the corresponding LFV cross section too small to be observable in the doubly-charged scalar fusion portal.[4] The flavor conserving process $e^+ e^- \to e^+ e^- H_3$ in Fig. 2 depends only on the coupling f_{ee} in the Yukawa

---

[4]Note that the low-energy rare decays $\mu \to eee$ and the production $ee \to e\mu H_3$ at high-energy lepton colliders have the same dependence on the combination of $|f_{ee}f_{e\mu}|/M_{\pm\pm}^2$ in the limit of heavy doubly-charged scalar mass. Thus, a lighter $H^{\pm\pm}$ pushes the limits on the $f_{\alpha\beta}$ couplings to more stringent values [note that the triple scalar coupling in Eq. (6) becomes smaller when the doubly-charged scalar gets lighter] and does not help to alleviate the limits from the LFV decays.
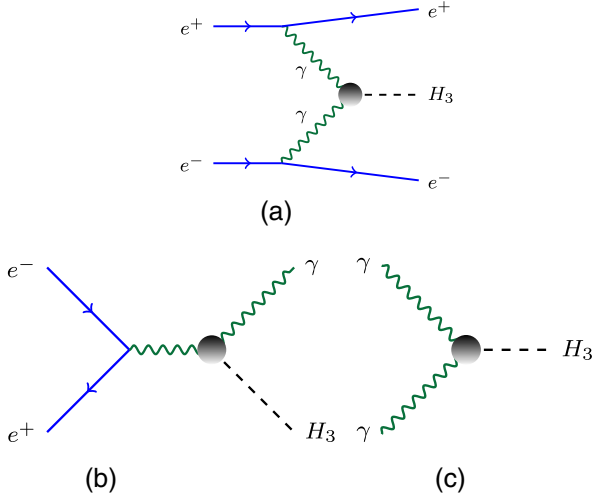
FIG. 4. Feynman diagrams for the production of H_3 at lepton colliders from the effective radiative coupling to photons (denoted by the black blob) in the process (a) $e^+e^- \to e^+e^-H_3$, (b) $e^+e^- \to \gamma H_3$ and (c) $\gamma\gamma \to H_3$.
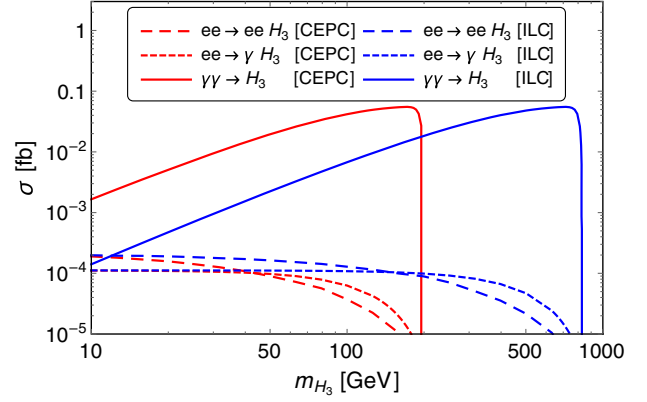

FIG. 5. Production cross section contours of H_3 at CEPC 240 GeV (red) and ILC 1 TeV (blue) from the radiative couplings to photons (see Fig. 4), as functions of the scalar mass m_{H_3}. The p_T cuts on the electrons and photons are all taken to be 5 GeV and the RH scale $v_R = 5$ TeV.

sector and is thus free of the LFV decay limits. It also contributes to Bhabha scattering and is constrained by the LEP $ee \to ee$ data [97], which are shown in Fig. 3 by the shaded region. The production cross section contours of $\sigma(ee \to eeH_3)$ are also presented in Fig. 3, as functions of the doubly-charged scalar mass $M_{\pm\pm}$ and $|f_{ee}|$ in the limit of small m_{H_3}. It is clear that even if the doubly-charged scalar is heavier than 1 TeV, there is still an ample parameter region to have an observable production cross section (up to 0.03 fb) that is allowed by the existing limits from LEP.

D. Gauge portal

The scalar H_3 can also be produced from the radiative couplings to photons, mediated by the heavy scalar and gauge bosons, as shown in Fig. 4. All the diagrams in Fig. 4 are effectively suppressed by the RH scale v_R, which is typically (much) higher than the center-of-mass energy. The cross section of photon fusion channel $\gamma^*\gamma^* \to H_3$ [Fig. 4(a)] depends largely on the momentum of the leptons in the final state: if the transverse momenta of the outgoing electron/positron are small, then the cross section would rise significantly like in Compton scattering. With an aggressive cut of $p_T(e^\pm) = 1$ GeV, the photon fusion cross sections are respectively 2.3×10^{-4} fb and 5.1×10^{-4} fb at CEPC 240 GeV and ILC 1 TeV, in the light H_3 limit for the RH scale $v_R = 5$ TeV. If the cuts are more realistic, like $p_T > 5$ GeV, the cross section is smaller, for instance $7.0 \times 10^{-5}(2.1 \times 10^{-4})$ fb at $\sqrt{s} = 240$ GeV (1 TeV), as shown in Fig. 5 (the long-dashed curves). The production cross section $\sigma(e^+e^- \to \gamma H_3)$ is also very small, roughly 1.1×10^{-4} fb in the light H_3 limit at both CEPC 240 GeV and ILC 1 TeV, with a $p_T > 5$ GeV cut on

the photon, which is also presented in Fig. 5. Even though the production cross sections would go larger as $\propto 1/v_R^2$ when the RH scale is to some extent lower, they are still too small.

In future lepton colliders, high luminosity photon beams can be obtained by Compton backscattering of a low-energy, high-intensity laser beam off the high-energy electron beam, and then H_3 can be produced from the laser "photon fusion" processes as shown in Fig. 4(c). The effective photon luminosity distribution reads [98–100]

$$f_{\gamma/e}(x) = \frac{1}{D(\xi)}\left[(1-x)+\frac{1}{(1-x)}-\frac{4x}{\xi(1-x)}+\frac{4x^2}{\xi^2(1-x)^2}\right],$$

with $D(\xi) = \left(1-\frac{4}{\xi}-\frac{8}{\xi^2}\right)\log(1+\xi)+\frac{1}{2}$ (9)

$$+\frac{8}{\xi}-\frac{1}{2(1+\xi)^2}, \quad\quad\quad (10)$$

where $x = \omega/E_e$ is the fraction of electron energy carried away by the scattered photon, with ω and E_e respectively the energies of the scattered photon and initial electron. The parameter $\xi = 4\omega_0 E_e/m_e^2$ depends on the energy ω_0 of the initial laser photon. When $\xi \gtrsim 4.8$ the photon conversion efficiency drops drastically, as a consequence of the e^+e^- pair production from the laser photons and the photon backscattering, which sets an upper bound on the energy fraction $x < x_{\max} = \xi/(1+\xi) \simeq 0.83$. The production cross sections $\sigma(\gamma\gamma \to H_3)$ at $\sqrt{s} = 240$ GeV and 1 TeV are shown in Fig. 5. The cross section could reach up to 0.05 fb for the RH scale $v_R = 5$ TeV.

E. SM Higgs portal

At lepton colliders, the most important channel to produce the SM Higgs is through the so-called Higgsstrahlung process, i.e., in association with a SM Z boson. If H_3 mixes
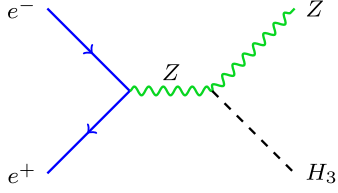
FIG. 6. Feynman diagram for the production of H_3 at lepton colliders from mixing with the SM Higgs.

with the SM Higgs, then it could be produced from the diagram in Fig. 6, with the amplitude proportional to the mixing angle $\sin\theta_1$. All the existing limits on the scalar mixing $\sin\theta_1$ are collected in Fig. 7. When H_3 is light, say lighter than the B meson masses, the mixing angle $\sin\theta_1$ is tightly constrained by the rare flavor-changing B meson decays like $B \to K\ell^+\ell^-$. For heavier H_3, the most stringent limit is from the $B_d - \bar{B}_d$ oscillation, which originates from the FCNC couplings of the heavy doublet scalar H_1 to the SM quarks and its mixing with the SM Higgs, which is governed by the VEV ratio κ'/κ in the bidoublet sector. See more details in Refs. [62,63]. In the limit of $m_B \ll m_{H_3}$ the B meson oscillation limit scales like $1/m_{H_3}^2$, as shown in Fig. 7. There are also constraints on the mixing angle from the precision Higgs data [101] and the direct searches of scalars at the LEP and LHC [86], which are however weaker than that from B_d oscillation data for the mass range $m_{H_3} < 1$ TeV.[5]

The total production cross section at the leading order can be easily obtained from that of the SM Higgs,

$$\sigma(e^+e^- \to ZH_3) = \frac{G_F m_Z^4 \sin^2\theta_1}{96\pi s}(v_e^2 + a_e^2)$$
$$\times \lambda^{1/2}\frac{\lambda + 12m_Z^2/s}{(1 - m_Z^2/s)^2}, \quad (11)$$

with $v_e = -1$, $a_e = -1 + 4\sin\theta_w$, and

$$\lambda = \left(1 - \frac{m_{H_3}^2}{s} - \frac{m_Z^2}{s}\right)^2 - \frac{4m_{H_3}^2 m_Z^2}{s^2}. \quad (12)$$

The production cross sections at CEPC 240 GeV and ILC 1 TeV are shown in Fig. 7 respectively as the red and blue contours, with the values of 0.1, 0.01 and 0.001 fb. Even if the flavor and direct search constraints are taken into consideration, for a wide range of H_3 masses, from 6 to 149 GeV (75 to 900 GeV), the production cross section is still larger than 0.01 fb at CEPC (ILC), excluding the vicinity of SM Higgs from roughly 120 to 130 GeV, with a clear signal of $e^+e^- \to ZH_3$ with $H_3 \to \gamma\gamma$ or H_3 decaying

---

[5]In models where the FCNC couplings to the SM quarks are loop induced, like a $U(1)_{B-L}$ gauge extension of the SM, the constraints from B oscillation data would be much weaker and the limits from Higgs precision data and direct searches at LEP and LHC take over as the primary constraints for a heavy scalar [63].
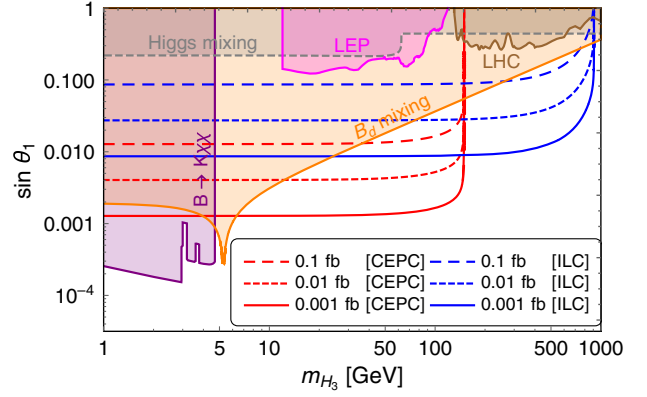

FIG. 7. Experimental limits on the mixing angle $\sin\theta_1$ of H_3 with the SM Higgs (with the mixing angle $\sin\theta_2$ set to zero), as a function of the scalar mass m_{H_3}: the flavor-changing decays $B \to K\chi\chi$ (purple), the $B_d - \bar{B}_d$ oscillation data (orange) [62,63], the Higgs precision measurements (gray) [101], the direct searches of scalars at the LEP (pink) and LHC (brown) [86]. For the B meson limits, the bidoublet VEV ratio $\xi = \kappa'/\kappa$ is set to be m_b/m_t as in Refs. [62,63]. All the shaded regions are excluded. The red and blue contours are respectively the production cross sections of 0.1 fb (long dashed), 0.01 fb (short-dashed) and 0.001 fb (solid) at CEPC 240 GeV and ILC 1 TeV, as functions of the scalar mass m_{H_3} and mixing angle $\sin\theta_1$.

into a pair of charged leptons with different flavors, as implied by Fig. 1.

F. Neutrino portal

In the LRSM, the tiny neutrino masses are generated via the type-I seesaw mechanism (and/or type-II seesaw). With the Dirac and Majorana mass matrices m_D and M_N, the heavy and light neutrinos could mix with each other, and the Feynman diagram in Fig. 8 can lead to production of an H_3. For $\mathcal{O}(1)$ Yukawa couplings $f_{\alpha\beta}$, the heavy neutrino masses $M_N \simeq 2f v_R$ are expected to be at the TeV scale (for the few-TeV scale v_R), and their mixing with the active neutrino $V_{\nu N} \sim 10^{-6}$. However, with specific textures of the matrices m_D and M_N, (some of) the heavy-light neutrino mixing angles might be sizable [78,83], or one or two of the RHNs masses could be much smaller than the RH scale, say at the GeV scale [40,102,103]. The production cross
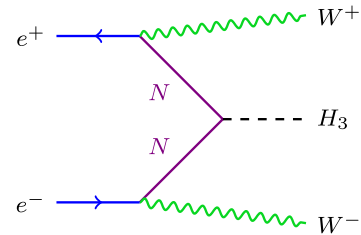

FIG. 8. Feynman diagram for the production of H_3 at lepton colliders from heavy-light neutrino mixing.
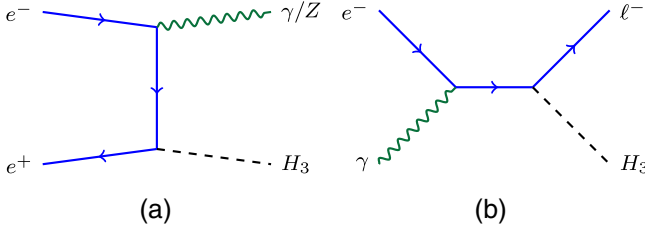
FIG. 9. Feynman diagrams for the on-shell production $e^+e^- \to (\gamma/Z)H_3$ (a) and $e^\pm\gamma \to \ell^\pm H_3$ (b) from the (LFV) couplings $h_{\alpha\beta}$ in Eq. (4).

section via the neutrino portal is, however, suppressed by both the heavy-light neutrino mixing $V_{\nu N}^4$ and the small Yukawa couplings $f^2 = (M_N/2v_R)^2$ in the LRSM when the RHN is light; therefore there is no hope to see the neutral scalar H_3 or to set any limits on the neutrino mixing by producing off-shell RHNs as in Fig. 8.

G. Heavy scalar portal

The $h_{\alpha\beta}$ couplings in Eq. (4) will induce the on-shell production processes $e^+e^- \to (\gamma/Z)H_3$, $e\gamma \to \ell H_3$ and $e^+e^- \to (\ell_\alpha^+\ell_\beta^-/\nu_\alpha\bar{\nu}_\beta)H_3$ as well as the off-shell processes $e^+e^- \to \ell_\alpha^+\ell_\beta^-$ [47], as aforementioned and detailed below.

1. On-shell production

The diagram for $e^+e^- \to (\gamma/Z)H_3$ is shown in Fig. 9(a), where we have neglected the mixing of H_3 with the SM Higgs and the loop-induced coupling of $H_3\gamma\gamma$. The amplitude is proportional to the effective coupling h_{ee} in Eq. (4). For illustration purposes, we show in the left panel of Fig. 10 the cross sections of $\sigma(e^+e^- \to (\gamma/Z)H_3)$ at the CEPC 240 GeV and ILC 1 TeV, as a function of the scalar mass m_{H_3}, for the value of $h_{ee} = 0.01$. Though the production of H_3 proceeds in this channel via the lepton flavor conserving coupling h_{ee}, the scalar H_3 could decay

into two charged leptons with different flavors, i.e., $H_3 \to \ell_\alpha^\pm\ell_\beta^\mp$ ($\alpha \neq \beta$), thus generating clear LFV signals.

The neutral scalar H_3 could also be produced in the process

$$e^\pm\gamma \to \ell^\pm H_3 (\ell = e, \mu, \tau), \qquad (13)$$

with the initial photon being the laser photon as in Sec. III D, and the flavor conversion "$e \to \ell$" induced by the coupling $h_{e\ell}$. The Feynman diagrams are shown in Fig. 9(b), and the corresponding cross sections at CEPC and ILC are presented in the right panel of Fig. 10, again with the value of $h_{e\ell} = 0.01$. Obviously the cross sections in the e^+e^- and $e\gamma$ channels are comparable to each other in a larger region of parameter space and largely complementary in probing the Yukawa couplings of H_3 at lepton colliders.

With the Yukawa couplings $h_{\alpha\beta}$ in Eq. (4), we can have the on-shell LFV processes of the form [47]

$$e^+e^- \to \ell_\alpha^\pm\ell_\beta^\mp H_3, \qquad \alpha \neq \beta, \qquad (14)$$

with the representative Feynman diagrams shown in the upper panels of Fig. 11. The neutral scalar H_3 can be emitted from any of the initial or final fermion lines in the Drell-Yan process $e^+e^- \to \ell^+\ell^-$ and hence potentially change the lepton flavors. The total production cross sections for $\ell_\alpha\ell_\beta = e\mu$ and $\mu\tau$ at CEPC 240 GeV and ILC 1 TeV are collected in the left panel of Fig. 12, with the nominal cuts of $p_T > 10$ GeV on the leptons. In a large parameter space the process $ee \to ee H_3$ is dominated by $ee \to Z H_3$ with the subsequent decay $Z \to ee$. The cross sections for $e\tau$ are almost the same as that for the $e\mu$, with subleading corrections from the muon and tauon mass difference, and are thus not shown in the plot. Only some of the diagrams in Fig. 11, e.g., the first one, apply to the process $ee \to \mu\tau + H_3$, and therefore the cross section for
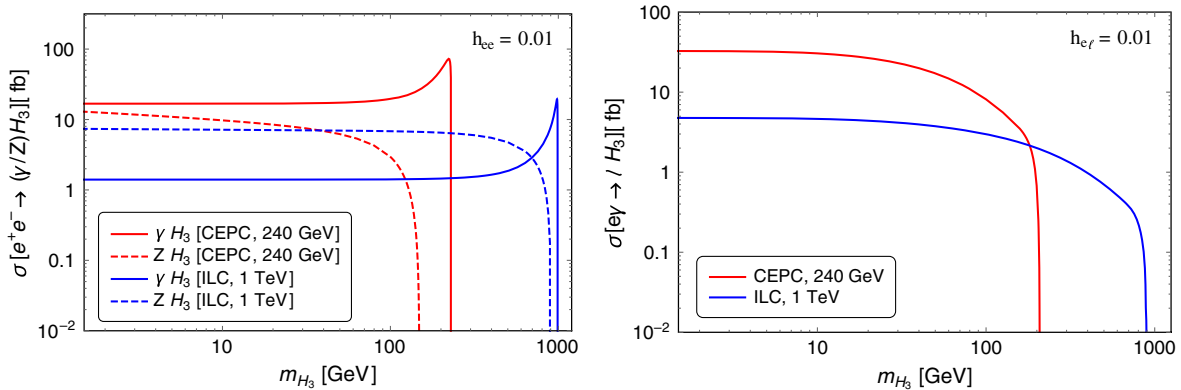

FIG. 10. Production cross sections of H_3 in the processes $e^+e^- \to (\gamma/Z)H_3$ (left) and $e^\pm\gamma \to \ell^\pm H_3$ (right) at CEPC 240 GeV (red) and ILC 1 TeV (blue), as functions of m_{H_3}, with the Yukawa coupling $h_{ee} = 0.01$ (left) or $h_{e\ell} = 0.01$ (right). For other values of h_{ee} or $h_{e\ell}$, the cross section can be simply rescaled by a factor of $(h_{ee}/0.01)^2$ (left) or $(h_{e\ell}/0.01)^2$ (right), though $h_{e\ell} = 0.01$ has been excluded for some ranges of m_{H_3} (see Fig. 18). See Fig. 9 for the diagrams.
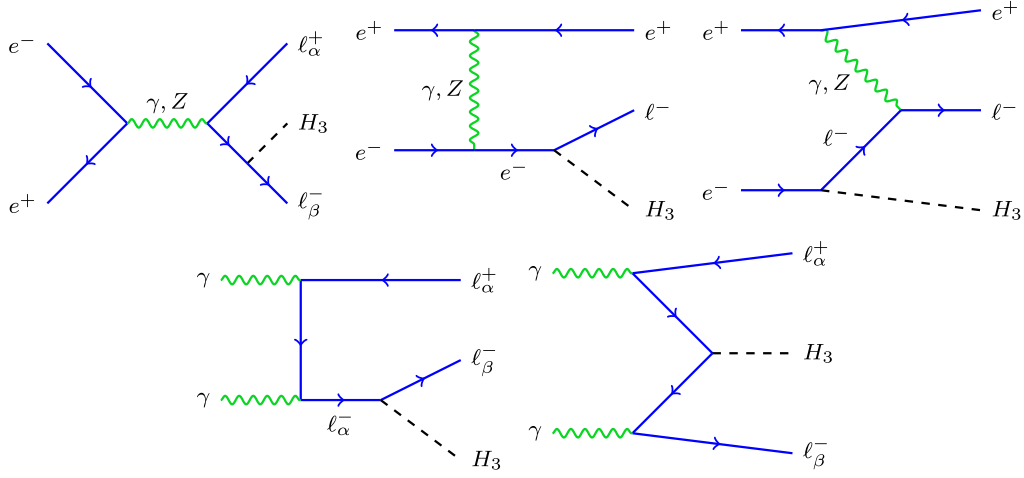
FIG. 11. Feynman diagrams for the on-shell production of H_3 via $e^+ e^- \to \ell_\alpha^+ \ell_\beta^- H_3$ (upper) and $\gamma\gamma \to \ell_\alpha^\pm \ell_\beta^\mp H_3$ (lower) at lepton colliders from the (LFV) couplings $h_{\alpha\beta}$ in Eq. (4).
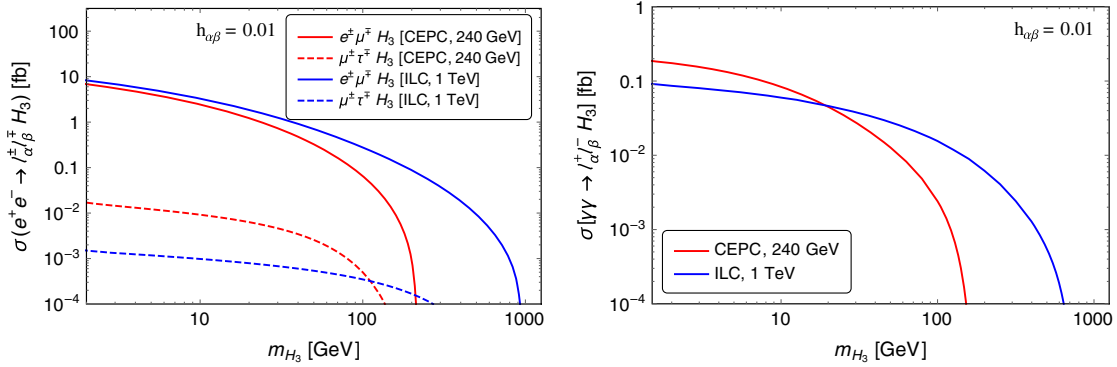

FIG. 12. Production cross sections of H_3 in the processes $e^+ e^- \to \ell_\alpha^\pm \ell_\beta^\mp H_3$ (with $\ell_\alpha \ell_\beta = e\mu, \mu\tau$, left) and $\gamma\gamma \to \ell_\alpha^+ \ell_\beta^- H_3$ (right) at CEPC 240 GeV (red) and ILC 1 TeV (blue), as functions of m_{H_3}. The Yukawa couplings involved $h_{\alpha\beta}$ are set to be 0.01 and all the others that are irrelevant are zero. For other values of $h_{\alpha\beta}$, the cross section can be simply rescaled by a factor of $(h_{\alpha\beta}/0.01)^2$, though $h_{\alpha\beta} = 0.01$ has been excluded for some ranges of m_{H_3} (see Fig. 18). See Fig. 11 for the diagrams.

the $\mu\tau$ channel is much smaller than those for $e\mu$ and $e\tau$, as clearly seen in Fig. 12. The cross sections with the final states $\mu\mu$ and $\tau\tau$ are approximately the same as that for $\mu\tau$.

H_3 could also be emitted from the $\gamma\gamma$ processes at lepton colliders, i.e.,

$$\gamma\gamma \to \ell_\alpha^\pm \ell_\beta^\mp H_3, \tag{15}$$

as shown in the lower panels of Fig. 11, and induce LFV signals if $\alpha \neq \beta$. The cross sections at CEPC and ILC are given in the right panel of Fig. 12, with the same cuts as above on the leptons. Note that for the final state with different flavors, e.g., $e^\pm \mu^\mp$, the cross section in Fig. 12 has to be multiplied by a factor of 2, to account for the two different flavor and charge combinations of $e^+ \mu^-$ and $e^- \mu^+$. The $\gamma\gamma$ processes could provide complementary prospects to those in Eq. (14) in searching for the LFV signals at future lepton colliders.

The neutral scalar H_3 could also be produced in the processes

$$e^+ e^- \to \nu_\alpha \bar\nu_\beta + H_3, \tag{16}$$

as shown in Fig. 13, with the flavors $\alpha = e$ or $\beta = e$ being induced from the LFV couplings $h_{\alpha\beta}$ in Eq. (4) if $\alpha \neq \beta$.
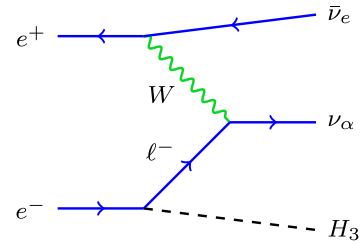

FIG. 13. Feynman diagram for the on-shell production of H_3 via $e^+ e^- \to \nu_\alpha \bar\nu_e H_3$ at lepton colliders from the (LFV) couplings $h_{\alpha\beta}$ in Eq. (4).
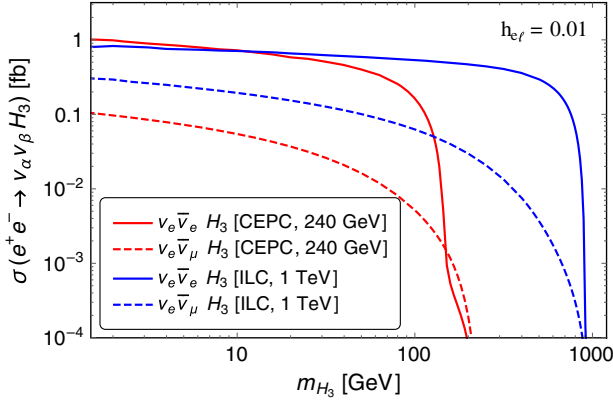
FIG. 14. Production cross sections of H_3 in the process of $e^+e^- \to \nu_\alpha \bar{\nu}_\beta H_3$ with $\nu_\alpha \bar{\nu}_\beta = \nu_e \bar{\nu}_e$ (solid) and $\nu_e \bar{\nu}_\mu$ (dashed) at CEPC 240 GeV (red) and ILC 1 TeV (blue), as functions of m_{H_3}. The Yukawa coupling involved (h_{ee} or $h_{e\mu}$) is set to be 0.01 and all the others that are irrelevant are zero. For other values of $h_{e\ell}$, the cross section can be simply rescaled by a factor of $(h_{e\ell}/0.01)^2$, though $h_{e\ell} = 0.01$ has been excluded for some ranges of m_{H_3} (see Fig. 18). See Fig. 13 for the diagram.

The production cross section for the cases of $\nu_e \bar{\nu}_e$ and $\nu_e \bar{\nu}_\mu$ (including also the contribution of $\nu_\mu \bar{\nu}_e$) at CEPC 240 GeV and ILC 1 TeV are presented in Fig. 14. It should be noted that for the case of $\nu_e \bar{\nu}_e$, there is extra contribution from the
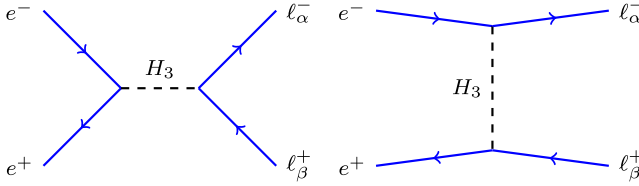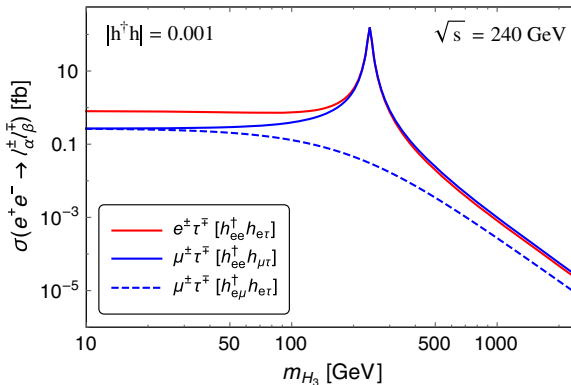

FIG. 15. Feynman diagrams for the off-shell production of H_3 via the process $e^+e^- \to \ell_\alpha^\pm \ell_\beta^\mp$ at lepton colliders from the (LFV) couplings $h_{\alpha\beta}$ in Eq. (4).

process $e^+e^- \to ZH_3$ with $Z \to \nu_e \bar{\nu}_e$, which cannot be distinguished from the W-mediated diagram in Fig. 13, as a result of the invisible nature of neutrinos. The solid red and blue lines in Fig. 14 combine both the contributions. If the vertex $H_3 \bar{e}\ell$ is flavor violating, i.e., $\ell = \mu$, τ, then we have only the diagram in Fig. 13, and the cross sections are comparatively smaller, as indicated by the dashed lines in Fig. 14. Neglecting the small charged lepton masses, the cross sections for $\nu_e \bar{\nu}_\tau$ are almost the same as that for $\nu_e \bar{\nu}_\mu$, and are thus not shown in Fig. 14.

2. Off-shell production

As studied in Ref. [47], even if the neutral scalar H_3 is heavier than the center-of-mass energy, the LFV signals could still be produced from an off-shell H_3, i.e.,

$$e^+e^- \to \ell_\alpha^\pm \ell_\beta^\mp, \tag{17}$$

with the diagram presented in Fig. 15. This could occur in both the s and t channels, depending on different combinations of the couplings $h_{\alpha\beta}$. For instance, the process $e^+e^- \to \mu^\pm \tau^\mp$ is respectively proportional to the couplings $|h_{ee}^\dagger h_{\mu\tau}|$ and $|h_{e\mu}^\dagger h_{e\tau}|$ in the s and t channels. The production cross sections for $e\tau$ and $\mu\tau$ (in both the s and t channels) are presented in Fig. 16, for the center-of-mass energies of 240 GeV and 1 TeV at CEPC and ILC, with the relevant couplings $|h^\dagger h| = 0.001$. In the s channel H_3 could be produced on shell if the colliding energy $\sqrt{s} \simeq m_{H_3}$, as clearly shown in the plots, where we have set explicitly the widths to be 10 and 30 GeV for CEPC and ILC, for the sake of concreteness.

H. Prospects at lepton colliders

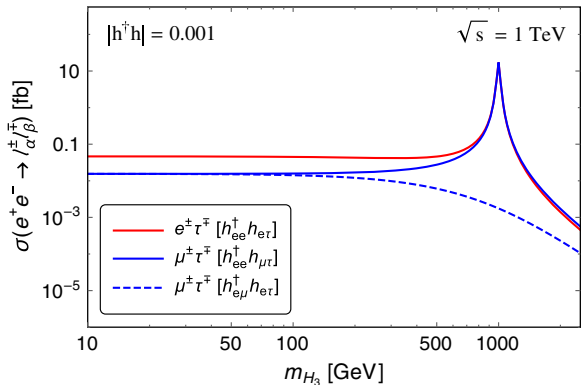In this section, we compare the future prospects of the neutral scalar search at lepton colliders in light of the

FIG. 16. Cross sections for the off-shell production of H_3 in the process $e^+e^- \to e^\pm \tau^\mp$, $\mu^\pm \tau^\mp$ from respectively the couplings $h_{ee}^\dagger h_{e\tau}$ (red); $h_{ee}^\dagger h_{\mu\tau}$ (blue, solid); and $h_{e\mu}^\dagger h_{e\tau}$ (blue, dashed) at CEPC 240 GeV (left) and ILC 1 TeV (right), as functions of m_{H_3}. The Yukawa coupling involved $|h^\dagger h|$ is set to be 10^{-3} and all the others that are irrelevant are zero. For other values of $|h^\dagger h|$, the cross section can be simply rescaled by a factor of $(|h^\dagger h|/10^{-3})^2$, though $|h^\dagger h| = 10^{-3}$ has been excluded for some ranges of m_{H_3} (see Fig. 19). See Fig. 15 for the diagrams.

existing constraints from both low- and high-energy sectors.

1. Current flavor constraints

The direct searches of neutral scalars have been performed at LEP [104] and LHC, e.g., when they decay into two SM fermions [105], gauge bosons [106–112], or di-Higgs [113–115], as already mentioned in Sec. III E. Here we summarize all the available flavor constraints on the Yukawa couplings $h_{\alpha\beta}$ in Eq. (4) [47,86], including those from the rare decays $\ell_\alpha \to \ell_\beta \ell_\gamma \ell_\delta$, $\ell_\alpha \to \ell_\beta \gamma$; the electron and muon $g - 2$; the muonium-antimuonium oscillation; and the LEP $e^+ e^- \to \ell^+ \ell^-$ data [97]. All the current experimental data and constraints on the couplings $h_{\alpha\beta}$ are collected in Table II.

In the limit of $m_{H_3} \gg m_\mu \gg m_e$, the partial decay width of $\mu \to eee$ is given by [120]

$$\Gamma(\mu^- \to e^+ e^- e^-) \simeq \frac{1}{\delta} \frac{|h_{ee}^\dagger h_{e\mu}|^2 m_\mu^5}{3072\pi^3 m_{H_3}^4}, \quad (18)$$

with the symmetry factor $\delta = 2$ accounting for the identical particles in the final state. The calculations of the widths for the LFV three-body tau decays such as $\Gamma(\tau^- \to e^+ e^- e^-)$ and $\Gamma(\tau^- \to \mu^- e^+ e^-)$ are quite similar, with the couplings and symmetry factor in Eq. (18) appropriately replaced.

The presence of couplings $h_{\alpha\beta}$ could induce the effective Wilson operators that couple the photon to an electron and muon at one-loop level,

$$\mathcal{O}_{\mu e\gamma, (L,R)} = \frac{e}{8\pi^2} m_\mu (\bar{e} \sigma^{\alpha\beta} P_{L,R} \mu) F_{\alpha\beta}, \quad (19)$$

with the effective coefficients, in the limit of $m_{H_3} \gg m_\tau \gg m_\mu \gg m_e$ [121,122],

$$c_L^{(\mu e\gamma)} = c_R^{(\mu e\gamma)}$$
$$\simeq \frac{1}{8 m_{H_3}^2} \left[\frac{1}{3} h_{ee}^\dagger h_{e\mu} + h_{e\mu}^\dagger h_{\mu\mu} \left(2 \log\left(\frac{m_{H_3}^2}{m_\mu^2}\right) - 3 \right) \right.$$
$$\left. + \frac{m_\tau}{m_\mu} h_{e\tau}^\dagger h_{\tau\mu} \left(2 \log\left(\frac{m_{H_3}^2}{m_\tau^2}\right) - 3 \right) \right]. \quad (20)$$

As expected, in the large m_{H_3} limit, the effective coefficients are suppressed by $m_{H_3}^2$. Then the partial decay width is

$$\Gamma(\mu \to e\gamma) = \frac{\alpha_{EM} m_\mu^5}{64\pi^4} (|c_L|^2 + |c_R|^2). \quad (21)$$

The calculations of $\Gamma(\tau \to e\gamma)$ and $\Gamma(\tau \to \mu\gamma)$ are quite similar, with m_μ^5 in Eq. (21) replaced by m_τ^5 and the corresponding Wilson coefficients

TABLE II. Current experimental data of the rare LFV decays $\ell_\alpha \to \ell_\beta \ell_\gamma \ell_\delta$, $\ell_\alpha \to \ell_\beta \gamma$ [76,116], the electron [117] and muon [118] $g - 2$, muonium oscillation [119] and the LEP $e^+ e^- \to \ell^+ \ell^-$ data [97], and the resultant constraints on the couplings $|h^\dagger h|/m_{H_3}^2$. Note that the $\ell_\alpha \to \ell_\beta \gamma$ and the electron and muon $g - 2$ constraints on $|h^\dagger h|/m_{H_3}^2$ have a weak dependence on the scalar mass m_{H_3}, due to the extra logarithm terms in Eqs. (20), (22)–(24). The $ee \to \ell\ell$ limits do not apply when $m_{H_3} \lesssim \sqrt{s}$. See text for more details.

Process	Current data	Constraints (GeV^{-2})
$\mu^- \to e^- e^+ e^-$	$< 1.0 \times 10^{-12}$	$\|h_{ee}^\dagger h_{e\mu}\|/m_{H_3}^2 < 6.6 \times 10^{-11}$
$\tau^- \to e^- e^+ e^-$	$< 1.4 \times 10^{-8}$	$\|h_{ee}^\dagger h_{e\tau}\|/m_{H_3}^2 < 1.9 \times 10^{-8}$
$\tau^- \to e^- \mu^+ \mu^-$	$< 1.6 \times 10^{-8}$	$\|h_{\mu\mu}^\dagger h_{e\tau}\|/m_{H_3}^2 < 1.4 \times 10^{-9}$
$\tau^- \to \mu^- e^+ \mu^-$	$< 9.8 \times 10^{-9}$	$\|h_{e\mu}^\dagger h_{\mu\tau}\|/m_{H_3}^2 < 1.5 \times 10^{-9}$
$\tau^- \to \mu^- e^+ e^-$	$< 1.1 \times 10^{-8}$	$\|h_{ee}^\dagger h_{\mu\tau}\|/m_{H_3}^2 < 1.2 \times 10^{-8}$
$\tau^- \to e^- \mu^+ e^-$	$< 8.4 \times 10^{-9}$	$\|h_{e\mu}^\dagger h_{e\tau}\|/m_{H_3}^2 < 1.4 \times 10^{-8}$
$\tau^- \to \mu^- \mu^+ \mu^-$	$< 1.2 \times 10^{-8}$	$\|h_{\mu\mu}^\dagger h_{\mu\tau}\|/m_{H_3}^2 < 1.7 \times 10^{-8}$
$\mu^- \to e^- \gamma$	$< 4.2 \times 10^{-13}$	$\|h_{ee}^\dagger h_{e\mu}\|/m_{H_3}^2 < 1.5 \times 10^{-9}$
		$\|h_{e\mu}^\dagger h_{\mu\mu}\|/m_{H_3}^2 < 2.1 \times 10^{-11}$
		$\|h_{e\tau}^\dagger h_{\tau\mu}\|/m_{H_3}^2 < 2.3 \times 10^{-12}$
$\tau^- \to e^- \gamma$	$< 3.3 \times 10^{-8}$	$\|h_{ee}^\dagger h_{e\tau}\|/m_{H_3}^2 < 1.0 \times 10^{-6}$
		$\|h_{e\mu}^\dagger h_{\mu\tau}\|/m_{H_3}^2 < 1.0 \times 10^{-6}$
		$\|h_{e\tau}^\dagger h_{\tau\tau}\|/m_{H_3}^2 < 2.6 \times 10^{-8}$
$\tau^- \to \mu^- \gamma$	$< 4.4 \times 10^{-8}$	$\|h_{\mu e}^\dagger h_{e\tau}\|/m_{H_3}^2 < 1.2 \times 10^{-6}$
		$\|h_{\mu\mu}^\dagger h_{\mu\tau}\|/m_{H_3}^2 < 1.2 \times 10^{-6}$
		$\|h_{\mu\tau}^\dagger h_{\tau\tau}\|/m_{H_3}^2 < 3.0 \times 10^{-8}$
Electron $g - 2$	$< 5.2 \times 10^{-13}$	$\|h_{e\mu}\|^2/m_{H_3}^2 < 6.2 \times 10^{-8}$
		$\|h_{e\tau}\|^2/m_{H_3}^2 < 6.9 \times 10^{-9}$
Muon $g - 2$	$< 4.0 \times 10^{-9}$	$\|h_{\mu\tau}\|^2/m_{H_3}^2 < 4.4 \times 10^{-7}$
Muonium oscillation	$< 8.2 \times 10^{-11}$	$\|h_{e\mu}^2\|/m_{H_3}^2 < 1.0 \times 10^{-7}$
$ee \to ee$ (LEP)	$\Lambda_{eff} > 5.7$ TeV	$\|h^\dagger h\|^2/m_{H_3}^2 < 1.9 \times 10^{-7}$
$ee \to \mu\mu$ (LEP)	$\Lambda_{eff} > 6.3$ TeV	$\|h^\dagger h\|^2/m_{H_3}^2 < 1.6 \times 10^{-7}$
$ee \to \tau\tau$ (LEP)	$\Lambda_{eff} > 7.9$ TeV	$\|h^\dagger h\|^2/m_{H_3}^2 < 1.0 \times 10^{-7}$

$$c_L^{(\tau e\gamma)} = c_R^{(\tau e\gamma)} \simeq \frac{1}{8 m_{H_3}^2} \left[\frac{1}{3} h_{ee}^\dagger h_{e\tau} + \frac{1}{3} h_{e\mu}^\dagger h_{\mu\tau} \right.$$
$$\left. + h_{e\tau}^\dagger h_{\tau\tau} \left(2 \log\left(\frac{m_{H_3}^2}{m_\tau^2}\right) - 3 \right) \right], \quad (22)$$

$$c_L^{(\tau\mu\gamma)} = c_R^{(\tau\mu\gamma)} \simeq \frac{1}{8 m_H^2} \left[\frac{1}{3} h_{\mu e}^\dagger h_{e\tau} + \frac{1}{3} h_{\mu\mu}^\dagger h_{\mu\tau} \right.$$
$$\left. + h_{\mu\tau}^\dagger h_{\tau\tau} \left(2 \log\left(\frac{m_{H_3}^2}{m_\tau^2}\right) - 3 \right) \right]. \quad (23)$$

The $H_3 - \mu$ and $H_3 - \tau$ loops contribute to the electron magnetic dipole moment, given by [123]

$$\Delta a_e \simeq \sum_{\ell=\mu,\tau} \frac{h_{e\ell}^2 m_e m_\ell}{16\pi^2 m_{H_3}^2} \left[2\log\left(\frac{m_{H_3}^2}{m_\ell^2}\right) - 3 \right]. \quad (24)$$

It is simple to get the extra contribution for the muon $g - 2$, which is dominated by the coupling $h_{\mu\tau}$.

The muonium-antimuonium oscillation probability is given by [124]

$$\mathcal{P} = \frac{2|\Delta M|^2}{\Gamma_\mu^2 + 4|\Delta M|^2} \quad (25)$$

with the H_3-induced mass splitting

$$|\Delta M| = \frac{2\alpha_{\text{EM}}^3 |h_{e\mu}|^2 \mu^3}{\pi m_{H_3}^2}, \quad (26)$$

with $\mu = m_e m_\mu/(m_e + m_\mu)$ the effective mass. In the denominator of Eq. (25), the muon decay width Γ_μ is typically much larger than $2|\Delta M|$ for the range of mass and couplings we are interested in; therefore, $\mathcal{P} \propto |h_{e\mu}|^4/m_{H_3}^4$.

The dimuonium (not yet found experimentally), i.e., the bound state $\text{Dm} \equiv (\mu^+\mu^-)$, could also be affected by the LFV couplings $h_{\alpha\beta}$ in Eq. (4), e.g., a t-channel H_3 could contribute to the decay $\text{Dm} \to e^+e^-$.[6] Even if Dm is found in the low-energy experiments and its decay BR into e^+e^- is consistent with the SM prediction, the theoretical uncertainties would imply a bound $|h_{e\mu}|^2/m_{H_3}^2 \lesssim \text{GeV}^{-2}$ [125–127], which is much weaker than the muonium oscillation constraint.

The neutral scalar H_3 could mediate the scattering $e^+e^- \to \ell^+\ell^-$ ($\ell = e, \mu, \tau$), in the s and/or t channel, depending on the couplings involved, e.g., the $ee \to \mu\mu$ could be induced in the s channel by the coupling $h_{ee}^\dagger h_{\mu\mu}$ and in the t channel by $h_{e\mu}$. The H_3-mediated diagrams interfere with the pure SM process, thus altering both the total cross section and differential distributions [128]. The LEP data exclude an effective cutoff scale Λ_{eff} of a few TeV, by analyzing the $ee \to \ell\ell$ data [97], which could be used to set limits on the couplings $\Lambda_{\text{eff}} \sim m_{H_3}/\sqrt{|h^\dagger h|}$, as collected in Table II. When H_3 is lighter than the center-of-mass energy $\sqrt{s}$, the limits on the effective cutoff scale Λ_{eff} do not apply, and we have to consider the H_3 propagator:

$$\frac{1}{q^2 - m_{H_3}^2} = \frac{1}{-s\cos\theta/2 - m_{H_3}^2}. \quad (27)$$

For simplicity we take an average over the scattering angle $\langle\cos\theta\rangle \simeq 1/2$ to interpret the LEP constraints. Then in the

---

[6]If $m_{H_3} \lesssim m_\mu$, then Dm could also decay via $\text{Dm} \to H_3 H_3$, which would turn out to be invisible if $|h_{ee}|$ is sufficiently small such that the decay length of $H_3 \to e^+e^-$ is long enough at the detector level.

limit of $m_{H_3} \ll \sqrt{s}$, the propagator is dominated by the q^2 term, and the $ee \to \ell\ell$ limit in Figs. 18 and 19 approaches a constant, as expected.

2. Comparison of different production portals

All the Feynman diagrams of H_3 production through its couplings to leptons, scalars and gauge bosons (including also the loop-level coupling to photons) at future e^+e^- colliders can be found in Figs. 2, 4, 6, 8, 9, 11, 13 and 15. Categorizing by the particles in the final state, all these production channels are collected in Table III. For the associated production of $H_3 Z$, we include only the visible decays of the Z boson, while the invisible decays of $Z \to \nu\bar{\nu}$ are categorized into the channel with large missing energy $H_3 + \not{E}_T$.

It should be noted that for some of the production channels, we can have more than one portal depending on the different couplings in the Lagrangian (4). For instance, the associated production with a pair of leptons $H_3 \ell_\alpha^\pm \ell_\beta^\mp$ can be induced from the trilinear scalar coupling to the doubly-charged scalars $H^{\pm\pm}$ (Fig. 2), from the fusion of photons if $\ell_\alpha^\pm \ell_\beta^\mp = e^+e^-$ via the loop-level effective coupling $H_3\gamma\gamma$ [Fig. 4(a)], from the (LFV) couplings $h_{\alpha\beta}$ to the charged leptons (Fig. 11), or from the process $H_3 Z$ with the subsequent decay $Z \to \ell^+\ell^-$ if $\alpha = \beta$ [Fig. 9(a)]. In most of the parameter space, it is likely that one (or more) of the portals will dominate, depending largely on the relevant parameters. In some cases, the kinematic distributions of the final states might also be used to distinguish different production portals. A thorough comparison of all the portals

TABLE III. Production channels of H_3 at future e^+e^- colliders, and the corresponding Feynman diagrams. See text for more details.

| Channel	Diagram(s)	Comment
H_3	Fig. 4(c)	Loop coupling to photons
$H_3 \ell_\alpha^\pm$	Fig. 9(b)	(LFV) couplings to $\ell^\pm$
$H_3 + \not{E}_T$	Fig. 13	(LFV) couplings to $\ell^\pm$
	Figs. 6, 9(a)	From $H_3 Z$, $Z \to \nu\bar{\nu}$
$H_3\gamma$	Fig. 4(b)	Loop coupling to photons
	Fig. 9(a)	Coupling to $e^\pm$
$H_3 Z$ ($Z \to$ visible)	Fig. 6	Mixing with SM Higgs
	Fig. 9(a)	Coupling to $e^\pm$
$H_3 W^+ W^-$	Fig. 8	Couplings to RHNs
$H_3 \ell_\alpha^\pm \ell_\beta^\mp$	Fig. 2	Coupling to $H^{\pm\pm}$
	Fig. 4(a)	Loop coupling to photons ($\ell_\alpha^\pm \ell_\beta^\mp = e^+e^-$)
	Fig. 11	(LFV) couplings to $\ell^\pm$
	Figs. 6, 9(a)	From $H_3 Z$, $Z \to \ell^+\ell^-$ ($\alpha = \beta$)
$\ell_\alpha^\pm \ell_\beta^\mp$	Fig. 15	Off-shell production
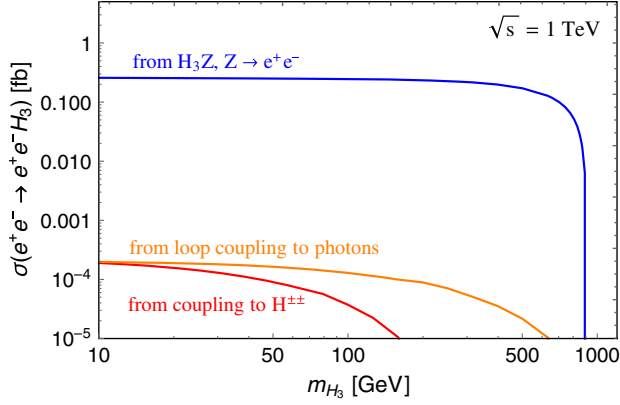
FIG. 17. Production cross sections of H_3 in the process of $e^+e^- \to e^+e^-H_3$ at ILC 1 TeV from coupling to the doubly-charged scalar $H^{\pm\pm}$ (red), from the loop-level coupling to photons (orange) and from the process H_3Z in Fig. 9(a) with the subsequent decay $Z \to e^+e^-$ (blue), as functions of m_{H_3}, with the benchmark parameters in Eq. (28).

for the processes in Table III goes beyond the main scope of this work. However, for illustration purposes we present the production cross sections $\sigma(e^+e^- \to e^+e^-H_3)$ in Fig. 17 from all the scalar, gauge and H_3Z ($Z \to e^+e^-$) portals collected in Table III, with the benchmark values of the parameters

$$\sin\theta_1 = 0, \qquad M_{\pm\pm} = 1 \text{ TeV},$$
$$f_{ee} = 0.2, \qquad h_{ee} = 0.01. \qquad (28)$$

Note that in the H_3Z process we have set the $h - H_3$ mixing to be zero such that it receives only the contribution from the coupling $H_3e^+e^-$ as shown in Fig. 9(a), with subleading contribution from the diagrams $e^+e^- \to e^+e^-H_3$ in Fig. 11 which are induced by the same coupling $H_3e^+e^-$. For the parameters chosen in Eq. (28), the doubly-charged scalar portal is highly suppressed by the mass $M_{\pm\pm}$ (red line in Fig. 17), while the gauge portal is highly suppressed by the loop-induced effective $H_3\gamma\gamma$ coupling (orange line in Fig. 17), and the process $e^+e^- \to e^+e^-H_3$ is dominated by the associated H_3Z production with the subsequent decay $Z \to e^+e^-$ (blue line in Fig. 17).

3. Prospects and LFV signals

All the amplitudes for the on-shell production of H_3 depend linearly on the couplings $h_{\alpha\beta}$, as shown in Figs. 9, 11 and 13, thus free of the constraints from the rare LFV decays such as $\mu \to eee$ and $\tau \to e\gamma$ which depend quadratically on the Yukawa couplings $|h^\dagger h|$, as clearly presented in Table II. With the production cross sections in Figs. 10, 12 and 14, one can readily estimate the prospects of all the independent couplings $h_{\alpha\beta}$ at future lepton colliders, which are collected in Fig. 18. As stated in Ref. [47], the SM backgrounds are expected to be small, in

particular for the LFV processes.[7] For simplicity, we have turned on only one of the couplings $h_{\alpha\beta}$ and set all others irrelevant to be zero. Neglecting the mixing of H_3 with the SM Higgs, the v_R^2-suppressed loop-decay $H_3 \to \gamma\gamma$ and the decay $H_3 \to \nu\bar{\nu}$ suppressed by the heavy-light neutrino mixing $V_{\nu N}^4$, the neutral scalar H_3 decays predominantly into a pair of leptons, i.e., $H_3 \to \ell_\alpha^\pm \ell_\beta^\mp$. To be concrete, we assume a minimum number of 10 (30) for the signals with (without) LFV, and adopt an efficiency factor of 60% for the tau lepton [65]. In the process $e^+e^- \to ZH_3$, only the visible decay products of Z are taken into account for the prospects of h_{ee} in the first row panels of Fig. 18, with roughly a BR($Z \to$ visible) $\simeq 80\%$.

Regarding the flavor conserving coupling h_{ee}, there exist only constraints from the LEP data $ee \to ee$ [97] (the limit from electron $g - 2$ [117] is highly suppressed by the electron mass and thus not considered). Given an integrated luminosity of 5 ab^{-1} (1 ab^{-1}) at CEPC (ILC), the coupling h_{ee} could be probed up to the order of 10^{-4} (10^{-3}), orders of magnitude lower than the current LEP constraints, as seen in the first row panels of Fig. 18. With three particles in the final state, the cross sections (and future prospects) for $\gamma\gamma \to eeH_3$ and $e^+e^- \to \nu\bar{\nu}H_3$ are comparatively weaker than those with only two particles such as $e^+e^- \to \gamma H_3$ and $e\gamma \to eH_3$.

As in Ref. [47], the most stringent constraints on $h_{e\mu}$ come from the muonium oscillation [119], the electron $g - 2$ [117] and the LEP $ee \to \mu\mu$ data [97]. A broad range of the mass m_{H_3} and $h_{e\mu}$ can be probed in the channels of $e\gamma \to \mu H_3$, e^+e^-, $\gamma\gamma \to e\mu H_3$ and $ee \to \nu\bar{\nu}H_3$ at future lepton colliders, as shown in the second row of panels in Fig. 18. The case for $h_{e\tau}$ is quite similar, with the existing limits primarily from the electron $g - 2$ and $ee \to \tau\tau$ data, as presented in the third row of panels in Fig. 18.

The processes involving only the muon and tauon flavors in the final state are limited, i.e., $e^+e^- \to (\mu\mu, \mu\tau, \tau\tau)H_3$ and $\gamma\gamma \to (\mu\mu, \mu\tau, \tau\tau)H_3$, as shown in the last row of panels in Fig. 18. If $h_{ee} \neq 0$, we also have the contribution from $e^+e^- \to ZH_3$, $Z \to \mu\mu$, $\tau\tau$, which are not included in the

---

[7]A detailed analysis of the SM backgrounds for the LFV processes is outside the scope of this paper. As the neutral scalar H_3 is hadrophobic and its couplings to the charged leptons are relatively small (compared to the SM gauge couplings), the decay width of H_3 is expected to be very small. Therefore the decay products of H_3 should form a sharp peak over the continuum SM background, mostly due to the gauge boson decays, which improve further the distinguishability of the signals and backgrounds, as illustrated in Ref. [47]. For LFV processes such as $e^+e^- \to \mu^+e^-H_3$ with $H_3 \to \mu^-e^+$, we expect a peak in the μ^-e^+ invariant mass distribution for the signal, which is absent in the SM, although one could get the same $e^+e^-\mu^+\mu^-$ final state from ZZ decay. Similarly, for lepton flavor conserving processes, e.g., $e^+e^- \to e^+e^-H_3$ with $H_3 \to e^-e^+$, the e^+e^- invariant mass peak due to H_3 can in principle be distinguished from the $Z \to e^+e^-$ SM background, by putting an invariant mass cut to exclude the Z-pole region.
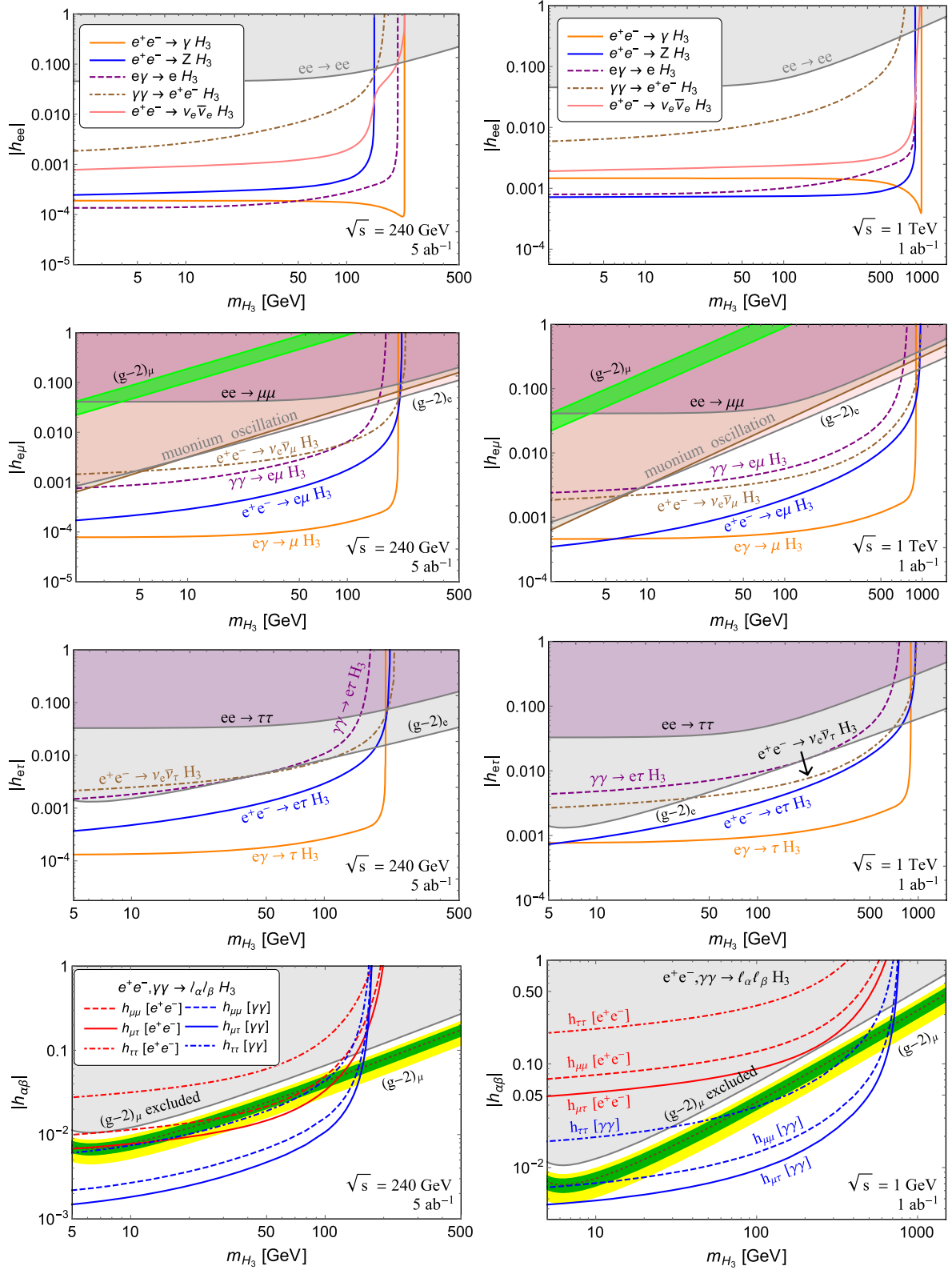
FIG. 18. Prospects of the couplings $h_{\alpha\beta}$ from the on-shell production of H_3 at CEPC (240 GeV and 5 ab^{-1}, left) and ILC (1 TeV and 1 ab^{-1}, right), in the channels of $e^+e^- \to (\gamma/Z)H_3$, $e\gamma \to \ell H_3$, e^+e^-, $\gamma\gamma \to \ell_\alpha^\pm \ell_\beta^\mp H_3$ and $e^+e^- \to \nu\bar{\nu}H_3$. The shaded regions are excluded by the muonium oscillation, electron $g-2$, muon $g-2$ (excluded by the theoretical-experimental discrepancy at the 5σ C.L.) [76] and the LEP $e^+e^- \to \ell^+\ell^-$ data [97], as indicated in Table II. The green and yellow bands in the second and fourth rows can explain the muon $g-2$ anomaly at the 1σ and 2σ C.L., respectively, while the dotted line at the center of the 1σ band corresponds to the central value.
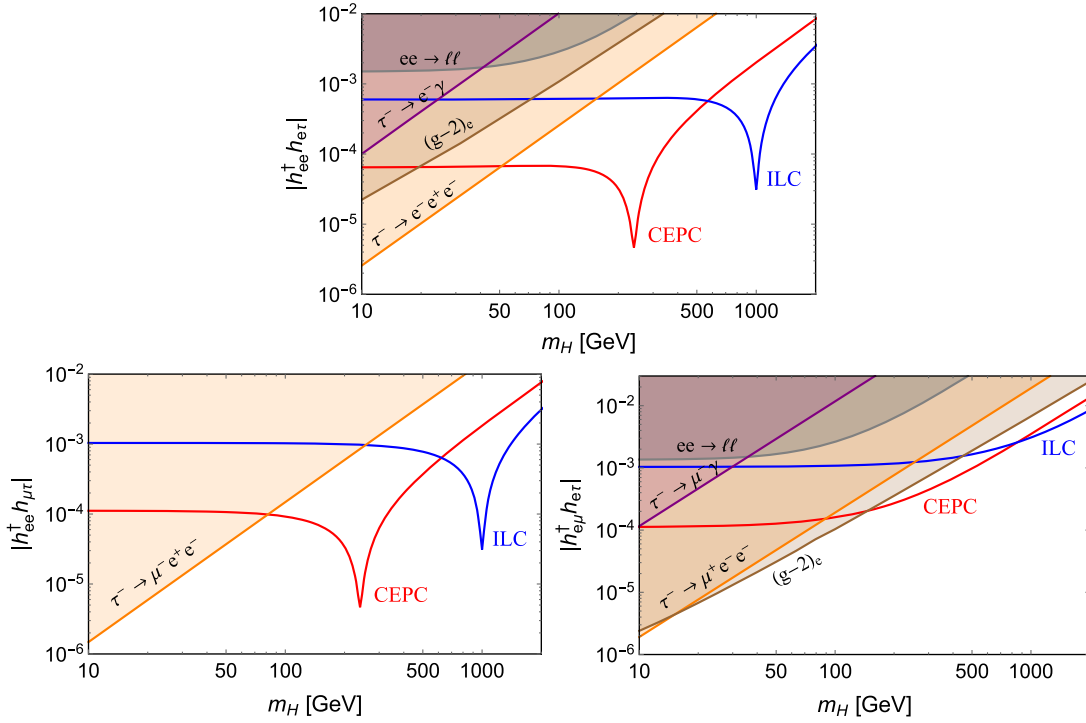
FIG. 19. Prospects of $|h^\dagger_{ee}h_{e\tau}|$ (upper), $|h^\dagger_{ee}h_{\mu\tau}|$ (lower left) and $|h^\dagger_{e\mu}h_{e\tau}|$ (lower right) from searches of $e^+e^- \to e^\pm\tau^\mp$, $\mu^\pm\tau^\mp$ at CEPC (red, $\sqrt{s} = 240$ GeV, $\mathcal{L} = 5$ ab^{-1}) and ILC (blue, 1 TeV and 1 ab^{-1}). Also shown are the constraints from the rare lepton decays $\ell_\alpha \to \ell_\beta\ell_\gamma\ell_\delta$, $\ell_\alpha \to \ell_\beta\gamma$, electron $g-2$ [76], and the LEP $e^+e^- \to \ell^+\ell^-$ data [97], as indicated (cf. Table II). The figure is from Ref. [47].

last two panels, as they do not depend on the couplings $h_{\mu\mu,\tau\tau}$. As a result of the smaller cross sections, the prospects for the couplings $h_{\mu\mu,\mu\tau,\tau\tau}$ are comparatively weaker than those for $h_{e\ell}$. However, the coupling $h_{\mu\tau}$ could provide a natural explanation for the muon $g-2$ anomaly [76]

$$\Delta a_\mu = (2.87 \pm 0.80) \times 10^{-9} \qquad (29)$$

in the presence of the neutral scalar H_3, as indicated by the green and yellow bands in the last two panels of Fig. 18 covering the 1σ and 2σ ranges respectively around the central value (dotted line). More importantly, it could be directly tested at the future lepton colliders like CEPC and ILC (and FCC-ee and CLIC), by searching for the LFV signals

$$e^+e^-, \gamma\gamma \to \mu^\pm\tau^\mp + H_3, \qquad (30)$$

with H_3 decaying back into $\mu - \tau$ pairs or other particles such as two photons (cf. the solid blue and red lines in the last two panels of Fig. 18). Almost the whole (kinematically allowed) parameter space could be covered, if a sizable BR of the H_3 decay products, say $\gtrsim 10\%$, could be reconstructed at lepton colliders.

As seen in Table II, the decay $\mu \to eee$ sets a very stringent limit on the coupling $|h^\dagger_{ee}h_{e\mu}|$; thus there is no

hope to see any signal of $e^+e^- \to e^\pm\mu^\mp$. In the τ lepton sector, the constraints from the LFV decays $\tau \to \ell_\alpha\ell_\beta\ell_\gamma$ are much weaker, which leaves us a large parameter space to probe by direct searches at future lepton colliders. In light of the large production cross sections in Fig. 16 and the small SM background [129,130], the couplings $|h^\dagger h|$ can be measured down to 10^{-4} (10^{-3}) at CEPC (ILC), as shown in Fig. 19 [47], well beyond the existing flavor limits in Table II. In the vicinity of $m_{H_3} \simeq \sqrt{s}$, the production cross sections are largely enhanced by the resonance effect, if H_3 could be produced in the s channel, as seen in the upper and lower left panels of Fig. 19. For the sake of concreteness, we have set the width of H_3 to be 10 GeV (30 GeV) at 240 GeV (1 TeV). Even if m_{H_3} is larger than the center-of-mass energy, the LFV signals would still reveal new physics beyond the SM, if they were found at the future lepton colliders.

IV. THE DOUBLY-CHARGED SCALAR

In this section, we study the production and detection prospects of the doubly-charged scalar $H^{\pm\pm}$ in the LRSM at future lepton colliders.

A. Current experimental constraints

We first examine the current experimental constraints from the direct same-sign dilepton searches at LHC

[131,132], the low-energy flavor constraints from rare LFV decays of charged leptons like $\ell_\alpha \to \ell_\beta \gamma$ and $\ell_\alpha \to \ell_\beta \ell_\gamma \ell_\delta$ [76], the anomalous magnetic moments of electron and muon, the LEP $e^+ e^- \to \ell^+ \ell^-$ data (with $\ell = e, \mu, \tau$, with the diagram shown in the left panel of Fig. 26) [97], and muonium-antimuonium oscillation [119], as in the neutral scalar case in Sec. III.

Following the Yukawa Lagrangian in Eq. (3), the doubly-charged scalar $H^{\pm\pm}$ is RH, i.e., coupling only to the RH charged leptons, with the decay width

$$\Gamma(H^{\pm\pm} \to \ell_\alpha^\pm \ell_\beta^\pm) \simeq \frac{S_{\alpha\beta} M_{\pm\pm} |f_{\alpha\beta}|^2}{8\pi}, \qquad (31)$$

where $\alpha, \beta = e, \mu, \tau$ run over all the three flavors, and $S_{\alpha\beta} = 1(2)$ for $\alpha = \beta$ ($\alpha \neq \beta$) is the symmetry factor. In the case where parity and $SU(2)_R$ breaking scales are decoupled [133],[8] the left-handed triplet Δ_L decouples in such models from the TeV scale physics, and the Yukawa couplings $f_{\alpha\beta}$ in Eq. (3) are not directly connected to the active neutrino masses and mixings like in type-II seesaw [134–138], and all the entries can in principle be totally free parameters.

Regarding the decay of $H^{\pm\pm}$, in the LRSM, it couples also to the heavy W_R boson, dictated by the gauge coupling g_R. The current K and B meson oscillation data require that the W_R boson be beyond roughly 3 TeV [88,139]; thus a TeV scale doubly-charged scalar could decay only into two off-shell heavy W_R bosons, which decay further into the SM quarks (plus charged leptons and heavy RHNs if kinematically allowed), with the partial width [140]

$$\Gamma(H^{\pm\pm} \to W_R^{\pm*} W_R^{\pm*}) \simeq \frac{1}{\pi^2} \int_0^{M_{\pm\pm}^2} dp \int_0^{(M_{\pm\pm}-\sqrt{p})^2} dq$$
$$\times \frac{M_{W_R} \Gamma_{W_R}}{(p - M_{W_R}^2)^2 + M_{W_R}^2 \Gamma_{W_R}^2}$$
$$\times \frac{M_{W_R} \Gamma_{W_R}}{(q - M_{W_R}^2)^2 + M_{W_R}^2 \Gamma_{W_R}^2} \Gamma_0, \qquad (32)$$

where $\Gamma_0 = \frac{M_{\pm\pm}^3}{16\pi v_R^2} \lambda^{1/2}(p, q, M_{\pm\pm}^2)$
$$\times \left(\lambda(p, q, M_{\pm\pm}^2) + \frac{12pq}{M_{\pm\pm}^4} \right), \qquad (33)$$

---

[8]Such models allow $SO(10)$ embedding of TeV scale W_R left-right models and are compatible with coupling unification. Parity becomes a symmetry called D-parity in $SO(10)$, a discrete symmetry that transforms $f \to f^c$, and is broken close to the GUT scale (by the VEV of a parity-odd singlet scalar field) well before the $SU(2)_R$ gauge symmetry breaks. The D-parity is different from the Lorentz parity, in the sense that Lorentz parity only interchanges the left-handed fermions with the right-handed ones, whereas the D-parity also interchanges the $SU(2)_L$ Higgs fields with the $SU(2)_R$ Higgs fields.

and $\quad \lambda(a, b, c) \equiv \left(1 - \frac{a}{c} - \frac{b}{c} \right)^2 - \frac{4ab}{c^2}. \qquad (34)$

For sufficiently small $f_{\alpha\beta}$ couplings which are of great interest for the prospects of the $f_{\alpha\beta}$ couplings at future lepton colliders, the RHNs are expected to be lighter than the W_R boson. Then taking into account all the decays $W_R \to q\bar{q}$ and $W_R \to \ell N$ leads to the width $\Gamma_{W_R} \simeq g_R^2 M_{W_R}/4\pi$.

The SM W boson mixes with the heavy W_R boson, but the mixing angle is highly suppressed by the mass ratio via [61,88]

$$\tan \zeta_W \simeq -\frac{g_R}{g_L} \frac{2\tan\beta}{1 + \tan^2\beta} \frac{m_W^2}{M_{W_R}^2}$$
$$\simeq -3.5 \times 10^{-5} \times \left(\frac{\tan\beta}{m_b/m_t} \right) \left(\frac{g_R}{g_L} \right) \left(\frac{M_{W_R}}{3 \text{ TeV}} \right)^{-2}, \qquad (35)$$

with $\tan\beta = \kappa'/\kappa$ the VEV ratio in the bidoublet sector which might also be small in light of the mass hierarchy $m_{b,\tau} \ll m_t$ in the SM fermion sector. Thus we neglect here also the decay $H^{\pm\pm} \to W^\pm W^\pm$. Due to the severe FCNC constraints on the heavy doublet scalars $M_{\phi_2} \gtrsim 10$ TeV [88], the decay $H^{\pm\pm} \to H^{\pm*} H^{\pm*}$ (with $H^\pm$ the singly-charged scalar from the heavy doublet) is also highly suppressed.

The BRs of 1%, 10%, 50%, 90% and 99% for the doubly-charged scalar decay into the same-sign leptons and the heavy W_R boson pairs are shown in Fig. 20, where for simplicity we do not consider any of the flavor dependence in Eq. (31) and have taken $g_R = g_L$ and the RH scale $v_R = 5$ TeV in Eq. (33). For the on-shell production of a doubly-charged scalar at future lepton colliders, the dilepton channel will dominate over the heavy W_R channel, as long as its mass is below 1 TeV and the Yukawa coupling $f \gtrsim 10^{-4}$. For the off-shell production $e^+ e^- \to \ell_\alpha^\pm \ell_\beta^\mp$

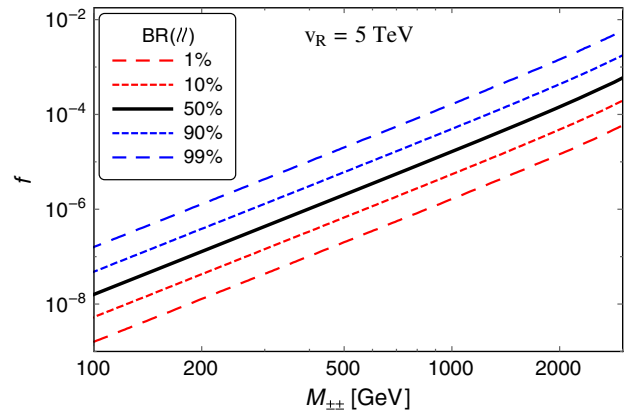FIG. 20. Contours of $\text{BR}(H^{\pm\pm} \to \ell_\alpha^\pm \ell_\beta^\pm) = 1 - \text{BR}(H^{\pm\pm} \to W_R^{\pm*} W_R^{\pm*}) = 1\%, 10\%, 50\%, 90\%, 99\%$ in the LRSM, as a function of the doubly-charged scalar mass $M_{\pm\pm}$ and the Yukawa coupling f. The gauge coupling $g_R = g_L$ and the RH scale $v_R = 5$ TeV.
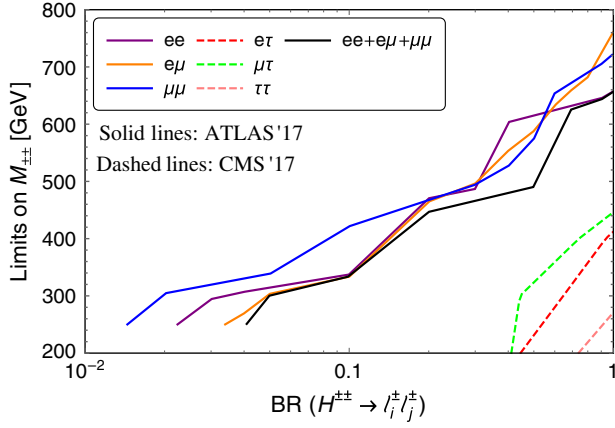
FIG. 21. Same-sign dilepton limits on the mass $M_{\pm\pm}$ of a RH doubly-charged scalar from ATLAS [131] (solid) and CMS [132] (dashed), as functions of BR($H^{\pm\pm} \to \ell_\alpha^\pm \ell_\beta^\pm$). The black solid line combines the three decay modes of ee, $e\mu$ and $\mu\mu$.

(see Fig. 26), as long as $M_{\pm\pm} < 2M_{W_R}$, the effects from the gauge coupling to the W_R boson could be neglected; otherwise for $M_{\pm\pm} > 2M_{W_R}$ it will contribute significantly to the total width of the doubly-charged scalar. Then the decay branching ratios into different flavor combinations of charged leptons are simply

$$\mathrm{BR}(H^{\pm\pm} \to \ell_\alpha^\pm \ell_\beta^\pm) = \frac{S_{\alpha\beta}|f_{\alpha\beta}|^2}{\sum_{\alpha,\beta}|f_{\alpha\beta}|^2}. \qquad (36)$$

The latest dilepton searches of $H^{\pm\pm} \to \ell_\alpha^\pm \ell_\beta^\pm$ at the LHC can be found in Refs. [131,132], with the doubly-charged scalar pair-produced form of the Drell-Yan process $pp \to \gamma^*/Z^* \to H^{++}H^{--}$. The limits on the doubly-charged scalar mass $M_{\pm\pm}$ for all six combinations of final states $ij = ee, e\mu, \mu\mu, e\tau, \mu\tau, \tau\tau$ are collected in Fig. 21, as well as the combined limit from $ee + e\mu + \mu\mu$, as functions of the corresponding BRs. For simplicity, we assume that only one of the six is open at a time and all the others are vanishing. The final states involving only the e and μ flavors are the most stringent [131] and those with the τ flavor are much weaker [132], as a result of the poor reconstruction efficiency of the τ lepton at hadron colliders. Note that all the limits in Ref. [132] are specific to the left-handed doubly-charged scalar; to interpret these limits onto the RH $H^{\pm\pm}$, we rescale down the pair-production cross section $\sigma(pp \to \gamma^*/Z^* \to H^{++}H^{--})$ by a factor of 2.3, to take into account the different couplings of left- and right-handed doubly-charged scalars to the Z boson.[9] All the

_____

[9]In the LRSM, the singly-charged scalar $H^\pm$ has an almost degenerate mass with the heavy neutral scalars H and A from the bidoublet, which is required to be beyond roughly 10 TeV by the flavor data [88]; thus the single production of $H^{\pm\pm}$ in associated production with $H^\pm$ is highly suppressed, and those single production data in [132] are not applicable to the LRSM, though the limits tend to be more stringent than the double production data.

limits in Figs. 5 and 6 of [132] for $H^{\pm\pm} \to e^\pm\tau^\pm$, $\mu^\pm\tau^\pm$, $\tau^\pm\tau^\pm$ have assumed a BR of 100% into each of the final states. To obtain the constraints in Fig. 21 as functions of the BRs, we rescale further down the theoretical predictions for the pair-production cross sections by a factor of BR[2]. For a doubly-charged scalar mass of 200 GeV, the BR for the final states involving the tauon flavor could go down to 0.45, 0.41 and 0.74 for respectively $e\tau$, $\mu\tau$ and $\tau\tau$, which is much weaker than the constraints from Ref. [131] with only electrons and muons, as expected: if the BRs get smaller, the production cross sections are too small to be constrained by the experimental data.

The LFV couplings $f_{\alpha\beta}$ (with $\alpha \neq \beta$) could induce rare flavor violating decays and anomalous magnetic moments which are highly suppressed in the SM. The partial width for the tree level three-body decay $\ell_\alpha \to \ell_\beta \ell_\gamma \ell_\delta$ is [141,142]

$$\mathrm{BR}(\ell_\alpha^- \to \ell_\beta^- \ell_\gamma^+ \ell_\delta^-)p \simeq \frac{|f_{\alpha\gamma}|^2|f_{\beta\delta}|^2}{2(1+\delta_{\beta\delta})G_F^2 M_{\pm\pm}^4}\mathrm{BR}(\ell_\alpha \to e\nu\bar{\nu}),$$
$$(37)$$

with G_F the Fermi constant and $\delta_{\beta\delta} = 1(0)$ for $\beta = \delta$ ($\beta \neq \delta$) the symmetry factor. As the doubly-charged scalar mass scale is much larger than the charged lepton masses, the constraints on $|f^\dagger f|/M_{\pm\pm}^2$ are almost constants, which correspond to an effective cutoff scale of $\Lambda \simeq M_{\pm\pm}/\sqrt{|f^\dagger f|}$. All the current experimental data on the rare muon and tauon decays and the corresponding upper limits on $|f^\dagger f|/M_{\pm\pm}^2$ are collected in Table IV.

At the one-loop level, the LFV couplings contribute to the two-body decays [143]

$$\mathrm{BR}(\ell_\alpha \to \ell_\beta\gamma) \simeq \frac{\alpha_{\mathrm{EM}}|\sum_\delta f_{\alpha\delta}^\dagger f_{\beta\delta}|^2}{3\pi G_F^2 M_{\pm\pm}^4} p\mathrm{BR}(\ell_\alpha \to e\nu\bar{\nu}), \quad (38)$$

where we have summed up all the diagrams involving a ℓ_δ lepton running in the loop. The experimental data of $\mu \to e\gamma$, $\tau \to e\gamma$ and $\tau \to \mu\gamma$ could be used to set limits on the couplings $|\sum_\delta f_{\alpha\delta}^\dagger f_{\beta\delta}|/M_{\pm\pm}^2$, which are also presented in Table IV. As a result of the loop factor, the constraints on the Yukawa couplings $|f^\dagger f|$ are one or two orders of magnitude weaker than those from the three-body decays $\ell_\alpha \to \ell_\beta \ell_\gamma \ell_\delta$, as shown in Table IV.

In an analogous way, we can calculate the contributions of the doubly-charged scalar loops to the anomalous magnetic moments of electron and muon (with $\alpha = e, \mu$) [144–146]:

$$\Delta a_\alpha \simeq -\frac{m_{\ell_\alpha}^2}{6\pi^2 M_{\pm\pm}^2}\sum_\beta |f_{\alpha\beta}|^2, \qquad (39)$$

where we have summed up the loops involving all three flavors $\beta = e, \mu, \tau$. The current 2σ experimental uncertainty

TABLE IV. Current experimental data of the rare LFV decays $\ell_\alpha \to \ell_\beta \ell_\gamma \ell_\delta$, $\ell_\alpha \to \ell_\beta \gamma$ [76,116], the electron [117] and muon [118] $g-2$, muonium oscillation [119] and the LEP $e^+ e^- \to \ell^+ \ell^-$ data [97], and the resultant constraints on the couplings $|f^\dagger f|/M_{\pm\pm}^2$ for the doubly-charged scalar.

Process	Current data	Constraints (GeV^{-2})
$\mu^- \to e^- e^+ e^-$	$< 1.0 \times 10^{-12}$	$|f_{ee}^\dagger f_{e\mu}|/M_{\pm\pm}^2 < 2.3 \times 10^{-11}$
$\tau^- \to e^- e^+ e^-$	$< 1.4 \times 10^{-8}$	$|f_{ee}^\dagger f_{e\tau}|/M_{\pm\pm}^2 < 6.6 \times 10^{-9}$
$\tau^- \to e^- \mu^+ \mu^-$	$< 1.6 \times 10^{-8}$	$|f_{e\mu}^\dagger f_{\mu\tau}|/M_{\pm\pm}^2 < 4.0 \times 10^{-9}$
$\tau^- \to \mu^- e^+ \mu^-$	$< 9.8 \times 10^{-9}$	$|f_{e\tau}^\dagger f_{\mu\mu}|/M_{\pm\pm}^2 < 5.2 \times 10^{-9}$
$\tau^- \to \mu^- e^+ e^-$	$< 1.1 \times 10^{-8}$	$|f_{e\mu}^\dagger f_{e\tau}|/M_{\pm\pm}^2 < 5.0 \times 10^{-9}$
$\tau^- \to e^- \mu^+ e^-$	$< 8.4 \times 10^{-9}$	$|f_{ee}^\dagger f_{\mu\tau}|/M_{\pm\pm}^2 < 5.5 \times 10^{-9}$
$\tau^- \to \mu^- \mu^+ \mu^-$	$< 1.2 \times 10^{-8}$	$|f_{\mu\mu}^\dagger f_{\mu\tau}|/M_{\pm\pm}^2 < 5.1 \times 10^{-9}$
$\mu^- \to e^- \gamma$	$< 4.2 \times 10^{-13}$	$|\sum_k f_{ek}^\dagger f_{\mu k}|/M_{\pm\pm}^2 < 2.7 \times 10^{-10}$
$\tau^- \to e^- \gamma$	$< 3.3 \times 10^{-8}$	$|\sum_k f_{ek}^\dagger f_{\tau k}|/M_{\pm\pm}^2 < 1.8 \times 10^{-7}$
$\tau^- \to \mu^- \gamma$	$< 4.4 \times 10^{-8}$	$|\sum_k f_{\mu k}^\dagger f_{\tau k}|/M_{\pm\pm}^2 < 2.1 \times 10^{-7}$
Electron $g-2$	$< 5.2 \times 10^{-13}$	$\sum_k |f_{ek}|^2/M_{\pm\pm}^2 < 1.2 \times 10^{-4}$
Muon $g-2$	$< 4.0 \times 10^{-9}$	$\sum_k |f_{\mu k}|^2/M_{\pm\pm}^2 < 1.7 \times 10^{-5}$
Muonium oscillation	$< 8.2 \times 10^{-11}$	$|f_{ee}^\dagger f_{\mu\mu}|/M_{\pm\pm}^2 < 1.2 \times 10^{-7}$
$ee \to ee$ (LEP)	$\Lambda_{\rm eff} > 5.2 \, {\rm TeV}$	$|f_{ee}|^2/M_{\pm\pm}^2 < 1.2 \times 10^{-7}$
$ee \to \mu\mu$ (LEP)	$\Lambda_{\rm eff} > 7.0 \, {\rm TeV}$	$|f_{e\mu}|^2/M_{\pm\pm}^2 < 6.4 \times 10^{-8}$
$ee \to \tau\tau$ (LEP)	$\Lambda_{\rm eff} > 7.6 \, {\rm TeV}$	$|f_{e\tau}|^2/M_{\pm\pm}^2 < 5.4 \times 10^{-8}$

$\Delta a_e = 5.2 \times 10^{-13}$ [76] can be used to set limits on the couplings $\sum_\beta |f_{e\beta}|^2$ as a function of the doubly-charged scalar mass. As the contributions from the doubly-charged scalar loops are always negative, the controversial theoretical and experimental discrepancy $\Delta a_\mu = (2.87 \pm 0.80) \times 10^{-9}$ cannot be explained; we use instead the 5σ uncertainty of $5 \times 0.80 \times 10^{-9}$ to constrain the Yukawa couplings, as shown in Table IV.

The muonium-antimuonium oscillation, i.e., the LFV conversion of the bound states $(\mu^+ e^-) \leftrightarrow (\mu^- e^+)$, can be induced by the effective four-fermion Lagrangian, which arises from the exchange of doubly-charged scalars in the LRSM [147]:

$$\mathcal{L}_{M\bar{M}} = \frac{G_{M\bar{M}}}{\sqrt{2}} [\bar{\mu}\gamma_\alpha(1+\gamma_5)e][\bar{\mu}\gamma^\alpha(1+\gamma_5)e] \qquad (40)$$

with the oscillation probability [124,148]

$$\mathcal{P} \simeq \frac{(\Delta M)^2}{2\Gamma_\mu^2}, \qquad (41)$$

where the mass splitting

$$\Delta M = 2\langle \bar{M}|\mathcal{L}_{M\bar{M}}|M\rangle = \frac{16 G_{M\bar{M}}}{\sqrt{2}\pi a^3}, \qquad (42)$$

with $a = (\alpha\mu)^{-1}$ and $\mu = m_e m_\mu/(m_e + m_\mu)$ the effective mass. By performing a Fierz transformation, the effective coefficient is related to the couplings and doubly-charged scalar mass via

$$G_{M\bar{M}} = \frac{f_{ee} f_{\mu\mu}^\dagger}{4\sqrt{2} M_{\pm\pm}^2}. \qquad (43)$$

The MACS experiment [119] sets a 90% C.L. upper bound of $\mathcal{P} < 8.2 \times 10^{-11}$, which requires that $|f_{ee}^\dagger f_{\mu\mu}|/M_{\pm\pm}^2 < 1.2 \times 10^{-7} \, {\rm GeV}^{-2}$, as shown in Table IV.

There are also direct searches of doubly-charged scalars at LEP in the single [149] or pair [150] production mode; limited by the center-of-mass energy, the constraints are very weak. An off-shell $H^{\pm\pm}$ in the t channel could mediate the Bhabha scattering $e^+ e^- \to e^+ e^-$ and interfere with the SM diagrams. This alters both the total cross section and the differential distributions [149,150]. If the Yukawa coupling f_{ee} is of order one, the doubly-charged scalar $H^{\pm\pm}$ could be probed up to the TeV scale. By Fierz transformation, the doubly-charged scalar contributes to the effective contact four-fermion interaction

$$\frac{1}{\Lambda_{\rm eff}^2}(\bar{e}_R \gamma_\mu e_R)(\bar{f}_R \gamma^\mu f_R), \qquad (44)$$

and it is constrained by the $ee \to \ell\ell$ (with $\ell\ell = ee$, $\mu\mu$, $\tau\tau$) data in Ref. [97]; $\Lambda_{\rm eff} \sim M_{\pm\pm}/|f_{e\ell}|$ corresponds to the effective cutoff scale related to the doubly-charged scalar mass and the Yukawa couplings. It turns out that the LEP data in Ref. [97] could provide more stringent limits than those in Refs. [149,150], so we list in Table IV only the limits on the cutoff scale $\Lambda_{\rm eff}$ from [97] and the consequent constraints on $|f_{e\ell}|^2/M_{\pm\pm}^2$.[10]

B. Production at colliders

1. Pair production

In the LRSM, the doubly-charged scalar $H^{\pm\pm}$ can be pair produced at lepton colliders through the Drell-Yan process and the Yukawa interaction $f_{e\ell}$ to the SM charged fermions [153], with ℓ covering all three flavors of e, μ and τ. The Feynman diagrams are shown in the upper panels of Fig. 22. At ILC, high luminosity photon beams can be obtained by Compton backscattering of a low-energy, high-intensity laser beam off the high-energy electron beam, and then the doubly-charged scalar can be pair produced from the "photon fusion" processes as shown in the lower panels

---

[10]For $f = e$, the effective interaction in Eq. (44) would also induce an additional contribution to the Møller scattering and can be constrained by the upcoming MOLLER experiment [151], which could probe the effective scale $\Lambda_{\rm eff} \simeq 5.3$ TeV, slightly stronger than the current limit from LEP data [152].
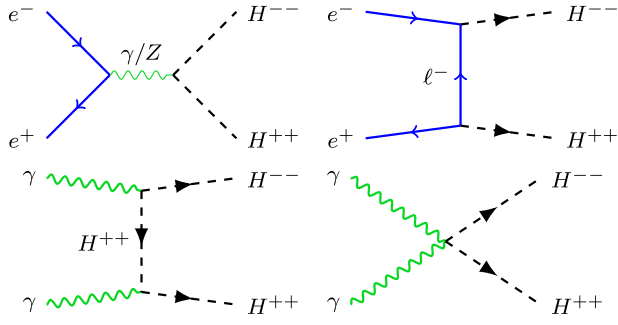
FIG. 22. Feynman diagrams for the pair production of a doubly-charged scalar $H_2^{\pm\pm}$ at lepton colliders through the Drell-Yan process (top left), the Yukawa couplings $f_{\alpha\beta}$ to the charged leptons (top right), and photon fusion (lower panels).

of Fig. 22 [154], including both the trilinear and quartic gauge-scalar couplings.[11] The effective photon luminosity distribution is given in Eq. (9) above [98–100].

The direct dilepton mass limits on the doubly-charged scalar mass $M_{\pm\pm}$ depend largely on the BRs of $H^{\pm\pm}$ decaying into different flavors of SM charged leptons; in particular, if $H^{\pm\pm}$ decays mostly into the tauon flavor, the same-sign dilepton limits are expected to be roughly below 440 GeV, as seen in Fig. 21, and $H^{\pm\pm}$ can be pair produced on shell at an ILC running of $\sqrt{s} = 1$ TeV (for the "photon fusion" process, the center-of-mass energy can only go effectively up to 1 TeV $\times\, x_{\max} \simeq 830$ GeV). The total cross sections at ILC 1 TeV for the pair production of doubly-charged scalars through the Drell-Yan process, the Yukawa couplings and the photon fusion are presented in Fig. 23. For concreteness, we have set $f_{ee} = 0.1$ and $f_{e\mu} = f_{e\tau} = 0$ in the Yukawa channel; for other specific values of the Yukawa couplings the cross section has to be rescaled by the factor of $|\sum_\ell f_{e\ell}|^2/0.1^4$. The electron/positron beams have been assumed to be unpolarized. For polarized beams, the cross section for the Yukawa coupling portal has to be rescaled by a factor of $(1 + P_{e^-})(1 - P_{e^+})$.

2. Single production

When the doubly-charged scalar is too heavy to be pair produced at lepton colliders, it could be singly produced from e^+e^- [153,156–158], $e\gamma$ [156,159–162] and $\gamma\gamma$ collisions, i.e.,[12]

---

[11]The doubly-charged scalar contributes to the light-by-light scattering at future lepton colliders and interferes with the SM processes; see e.g., Ref. [155].

[12]In the e^+e^- single production of a doubly-charged scalar, we have the subprocesses $e\gamma^* \to \ell_\alpha H^{\pm\pm}$, with the virtual photon emitted from the initial electron/positron [157,161] (see the second and third diagram in the upper row of Fig. 24), which is different from the laser photon in the $e\gamma$ collision in Eq. (45).
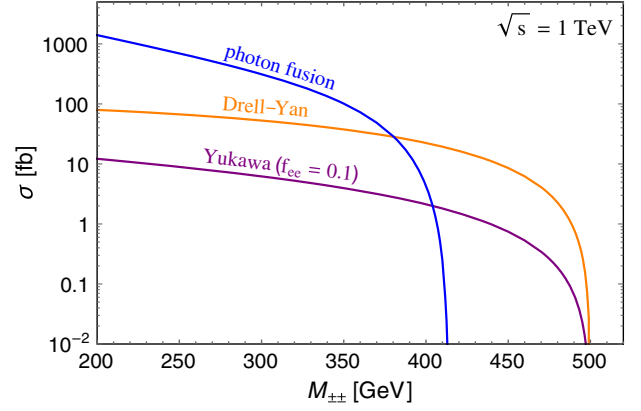

FIG. 23. Pair-production cross sections of the doubly-charged scalar $H^{\pm\pm}$ at ILC 1 TeV through the Drell-Yan process, the Yukawa couplings to the charged leptons (assuming $f_{ee} = 0.1$ and other couplings vanishing), and photon fusion. For other values of f_{ee}, the cross section in the Yukawa channel can be simply rescaled by a factor of $(f_{ee}/0.1)^2$, though $f_{ee} = 0.1$ has been excluded for some ranges of $M_{\pm\pm}$ (see Fig. 28). See Fig. 22 for the Feynman diagrams and text for more details.

$$e^+e^- \to H^{\pm\pm}\ell_\alpha^\mp \ell_\beta^\mp,$$
$$e^\pm\gamma \to H^{\pm\pm}\ell_\alpha^\mp,$$
$$\gamma\gamma \to H^{\pm\pm}\ell_\alpha^\mp \ell_\beta^\mp, \qquad (45)$$

with γ the laser photon beam as in the pair-production case. Some of the representative Feynman diagrams are shown in Fig. 24. For the e^+e^- single production, it is in fact the Drell-Yan process $ee \to \ell\ell$ with one doubly-charged scalar emitted from the initial or final state and possibly changing the lepton flavor [149]; see the first row of diagrams in Fig. 24. The process $e^+e^- \to H^{++*}H^{--}/H^{++}H^{--*}$ should also be taken into consideration, with one of the doubly-charged scalars in the final state on shell and the other one off shell (cf. the first diagram in Fig. 22). Similarly, for the $\gamma\gamma$ single production, we can have the doubly-charged scalar produced by couplings to the charged leptons in $\gamma\gamma \to \ell\ell$ (the lower row in Fig. 24) or with one off-shell doubly-charged scalar in the pair production like $\gamma\gamma \to H^{++*}H^{--}$ (cf. the last two diagrams in Fig. 22). The three diagrams in the middle row of Fig. 24 are examples for the single production $e^\pm\gamma \to H^{\pm\pm}\ell_\alpha^\mp$.

The cross sections for the single production of $H^{\pm\pm}$ depend largely on the production modes, the charged lepton flavors and the Yukawa couplings $f_{\alpha\beta}$ involved. Some representative production cross sections at ILC 1 TeV as functions of the doubly-charged scalar mass are presented in Fig. 25, with the nominal cuts of $p_T(\ell) > 10$ GeV and $|\eta(\ell)| < 2.5$. In particular, all the Yukawa couplings involved are assumed to be 0.1. When the scalar mass is roughly below $\sqrt{s}/2 = 500$ GeV, the signal of $H^{\pm\pm}\ell_\alpha^\mp \ell_\beta^\mp$
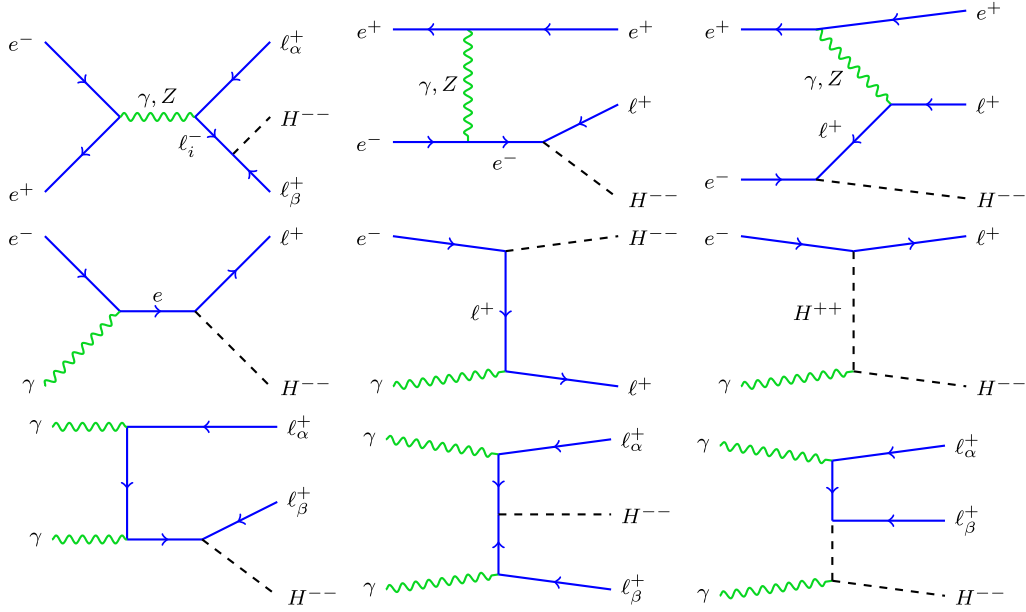
FIG. 24.   Representative Feynman diagrams for the single production of $H^{\pm\pm}$ at lepton colliders from the e^+e^- (upper), $e\gamma$ (middle) and $\gamma\gamma$ (lower) processes.

from both the e^+e^- and $\gamma\gamma$ processes would be dominated by the pair-production modes in Fig. 22, and the cross sections go much larger, as indicated by the thick black line in Fig. 25.

For the $e\gamma$ channel, the production cross sections are almost the same for the three flavors $\ell = e, \mu, \tau$ in the final state, up to the reconstruction efficiencies (in particular for the tauon lepton) and the Yukawa couplings, e.g., to obtain the cross section $\sigma(e^\pm\gamma \rightarrow H^{\pm\pm}\tau^\mp)$, one has only to multiply the
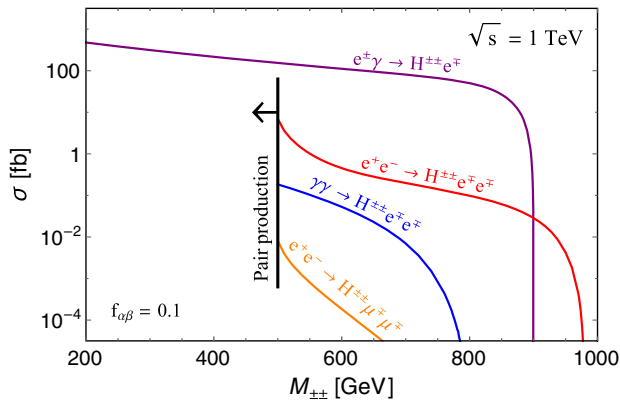

FIG. 25.   Single production cross sections of the doubly-charged scalar $H^{\pm\pm}$ at ILC 1 TeV through the e^+e^-, $e\gamma$ and $\gamma\gamma$ processes, with all the Yukawa couplings relevant set to be 0.1. On the left of the thick black line, the ee and $\gamma\gamma$ processes are dominated by the pair-production modes. For other values of $f_{\alpha\beta}$, the cross section can be simply rescaled by a factor of $(f_{\alpha\beta}/0.1)^2$, though $f_{\alpha\beta} = 0.1$ has been excluded for some ranges of $M_{\pm\pm}$ (see Fig. 28). See Fig. 24 for the Feynman diagrams and the text for more details.

corresponding value for $\sigma(e^\pm\gamma \rightarrow H^{\pm\pm}e^\mp)$ in Fig. 25 by a factor of $\epsilon_\tau \times |f_{e\tau}|^2/0.01$, with ϵ_τ the τ efficiency factor. One should note that due to $x_{max} \simeq 0.83 < 1$ for the laser photon, the center-of-mass energy could go only up to $(500 \text{ GeV}) \oplus (500 \text{ GeV} \times x_{max}) \simeq 911$ GeV. With the p_T cut of 10 GeV on the charged leptons, in reality the doubly-charged scalar mass could only be probed up to roughly 900 GeV, as shown in Fig. 25.

In the $e^+e^- \rightarrow H^{\pm\pm}\ell_\alpha^\mp\ell_\beta^\mp$ single production of $H^{\pm\pm}$, we can have all six distinct combinations of charged lepton flavors of α, β in the final state, i.e., $\ell_\alpha\ell_\beta = ee, e\mu, e\tau, \mu\mu, \mu\tau, \tau\tau$, which can be categorized into two groups: (a) those with an electron/positron in the final state ($ee, e\mu, e\tau$) and (b) those with only the muon or tauon flavors ($\mu\mu, \mu\tau, \tau\tau$). The production cross sections in each of the groups are roughly the same, up to the trivial symmetry factors for identical particles and the efficiency factors; two representative curves for ee and $\mu\mu$ are shown in Fig. 25. For instance, to obtain the cross section $\sigma(e^+e^- \rightarrow H^{\pm\pm}e^\mp\mu^\mp)$, one needs only to multiply that for an ee process by a factor of $2\epsilon_\mu \times |f_{e\mu}|^2$ with $\epsilon_\mu \simeq 1$ the muon efficiency factor. For the processes of the (b) group, only some of the diagrams in Fig. 24 contribute, e.g., the first one, and the cross sections are much smaller than those of the (a) group involving an $e^\pm$, as clearly seen in Fig. 25 by comparing the cross sections for ee and $\mu\mu$.

Regarding the production of a doubly-charged scalar in the process $\gamma\gamma \rightarrow H^{\pm\pm}\ell_\alpha^\mp\ell_\beta^\mp$, all the three lepton flavors are essentially on the same footing. In other words, all the fix different flavor combinations of $\ell_\alpha\ell_\beta$ share the same production cross sections as shown in Fig. 25 (in the plot we have explicitly set $\alpha\beta = ee$ and $f_{ee} = 0.1$), up to the
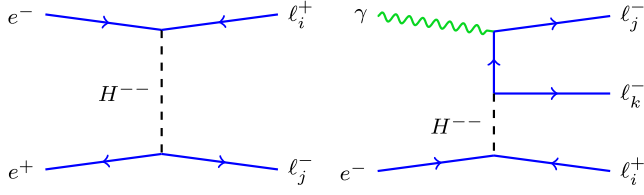
FIG. 26. Feynman diagrams for the off-shell production of $H^{\pm\pm}$ at lepton colliders from the e^+e^- (left) and $e\gamma$ (right) processes.

symmetry factors due to the identical particles $\alpha = \beta$, the Yukawa couplings $(f_{\alpha\beta}/0.1)^2$ and the efficiency factors.

3. Off-shell production

Even if the doubly-charged scalar is too heavy to be directly single/pair produced on shell at lepton colliders, it could still mediate the processes $e^+e^- \to \ell_\alpha^\pm \ell_\beta^\mp$ in the t channel [153] (if $\ell_\alpha \ell_\beta = e^+e^-$, then the doubly-charged scalar contributes to the Bhabha scattering), as shown in the left panel of Fig. 26, and induce LFV signals if $\alpha \neq \beta$. In an analogous way, we can have the trilepton processes $e^\pm \gamma \to \ell_\alpha^\mp \ell_\beta^\pm \ell_\gamma^\pm$ [159–161][13] with potential LFV signals if

$$\alpha\beta\gamma = ee\mu, ee\tau, e\mu\mu, e\mu\tau, e\tau\tau, \mu ee, \tau ee, \mu e\tau, \tau e\mu, \mu\mu\mu, \tau\tau\tau,$$

$$\mu\mu\tau, \tau\tau\mu, \mu\tau\tau, \tau\mu\mu, \tag{46}$$

as shown in the right panel of Fig. 26. As for the single production, here one has to take into account also the processes $e^\pm \gamma \to H^{\pm\pm*}\ell_\alpha^\mp \to \ell_\alpha^\mp \ell_\beta^\pm \ell_\gamma^\pm$ with the same-sign lepton pair ($\ell_\beta^\pm \ell_\gamma^\pm$) originating from the off-shell $H^{\pm\pm}$; cf. the diagrams in the middle row of Fig. 24.

For illustration purpose, we show in Fig. 27 the production cross sections for $e^+e^- \to e^\pm\mu^\mp$ and $e^\pm\gamma \to e^\mp e^- \mu^\pm$ at both CEPC 240 GeV and ILC 1 TeV. To be concrete, the Yukawa couplings involved have set to be $|f^\dagger f| = 0.01$, for instance $|f_{ee}^\dagger f_{e\mu}| = 0.01$ in the $e^\pm\mu^\mp$ channel (the solid and dashed purple curves in Fig. 27).

C. Prospects and LFV signals

Given the cross sections in the previous subsection for all the different modes of pair production, single production and off-shell production of the RH doubly-charged scalar $H^{\pm\pm}$ in the LRSM, we estimate the prospects for the doubly-charged scalar at future colliders like CEPC and ILC, in particular with the LFV signals which are highly suppressed in the SM. All the current LFV constraints are
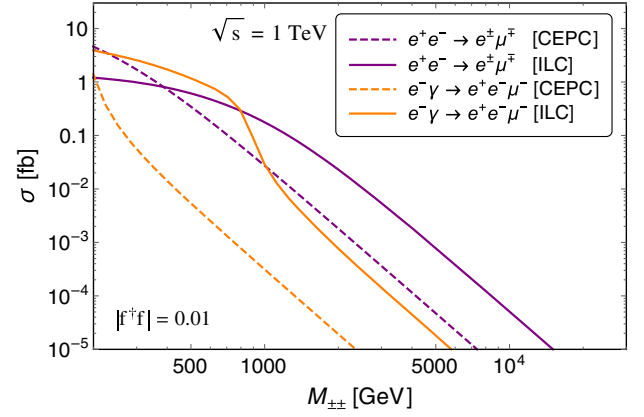

FIG. 27. Single production cross sections of the doubly-charged scalar $H^{\pm\pm}$ at CEPC (dashed, $\sqrt{s} = 240$ GeV) and ILC (solid, $\sqrt{s} = 1$ TeV) through the e^+e^- (purple) and $e\gamma$ (orange) processes, with all the Yukawa couplings $|f^\dagger f|$ relevant set to be 0.01. For other values of $|f^\dagger f|$, the cross section can be simply rescaled by a factor of $(|f^\dagger f|/0.01)^2$, though $|f^\dagger f| = 0.01$ has been excluded for some ranges of $M_{\pm\pm}$ (see Figs. 29 and 30). See Fig. 24 for the Feynman diagrams and text for more details.

collected in Table IV. One should note that some of the limits in Table IV depend on the products of two different entries in the Yukawa coupling matrix $f_{\alpha\beta}$, like the decays $\ell_\alpha \to \ell_\beta \ell_\gamma \ell_\delta$, $\ell_\alpha \to \ell_\beta \gamma$ and the muonium oscillation, while the $g - 2$ and LEP $e^+e^- \to \ell^+\ell^-$ data rely only on (combinations of) the single elements $f_{\alpha\beta}$.

Among all the on-shell and off-shell production modes in Sec. IV B, only the Drell-Yan process $e^+e^- \to H^{++}H^{--}$ and $\gamma\gamma \to H^{++}H^{--}$ do not depend on the Yukawa couplings $f_{\alpha\beta}$, but rather on the gauge couplings; cf. the first, third and fourth diagrams in Fig. 22. As stated in Sec. IV A, the doubly-charged scalar in the LRSM decays predominantly into the charged leptons, with the BR and flavor dependence given in Eq. (36). By counting the event numbers of different lepton flavors, one could, at least in principle, fix the *relative* magnitudes of the elements $f_{\alpha\beta}$, e.g., the ratios $|f_{\alpha\beta}|^2/|f_{ee}|^2$.[14] The absolute values of $f_{\alpha\beta}$ have to been determined from other on-shell channels.

At the leading order, both the amplitudes of the Yukawa pair production (the second diagram in Fig. 22) and single production channels in Fig. 24 are linear functions of the couplings $f_{\alpha\beta}$. In the simplest case with only one independent element of the f matrix turned on, one can predict

---

[13]It is also possible to have the off-shell production mode $\gamma\gamma \to \ell_\alpha^\pm \ell_\beta^\pm \ell_\gamma^\mp \ell_\delta^\mp$ with potentially LFV in the final state, but the cross sections are much smaller than the ee and $e\gamma$ processes and are thus not considered here.

[14]In the left-right models, in the limit of small $W - W_R$ mixing and heavy W_R boson, with sufficiently small Yukawa couplings $f_{\alpha\beta}$, the same-sign leptons from doubly-charged scalar decay will form displaced vertices [163], which is expected to be a strikingly clear signal at lepton colliders. The decay length of a doubly-charged scalar could, in principle, be used to determine the values of Yukawa couplings $|f_{\alpha\beta}|$ for a given doubly-charged scalar mass.
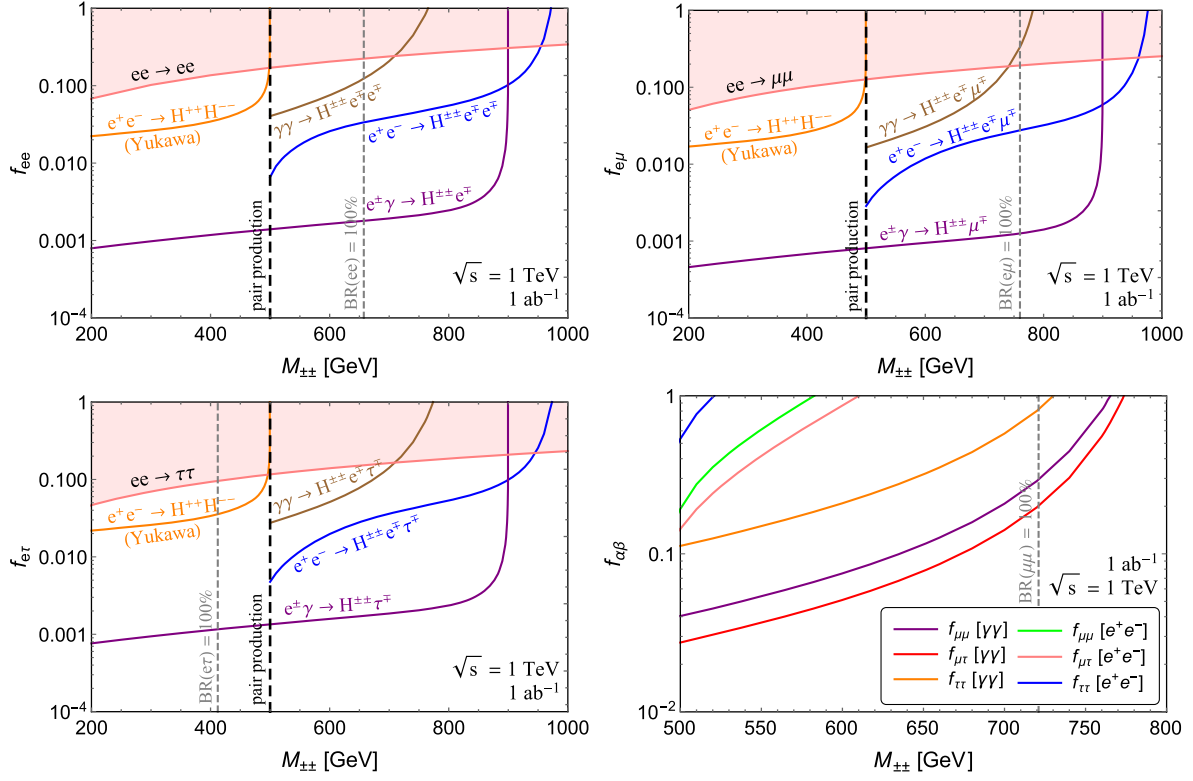
FIG. 28. Prospects of the doubly-charged scalar $H^{\pm\pm}$ at ILC 1 TeV and an integrated luminosity of 1 ab^{-1}. The top left, top right and bottom left panels show both the prospects in the Yukawa pair (orange) and single production modes of the e^+e^- (blue), $e\gamma$ (purple) and $\gamma\gamma$ (brown) processes, for respectively the couplings f_{ee}, $f_{e\mu}$ and $f_{e\tau}$, as functions of the doubly-charged scalar mass. The pink shaded regions are excluded by the LEP $ee \to \ell\ell$ data [97]. The prospects for the Yukawa couplings $f_{\alpha\beta}$ not involving the electron flavor are collected in the lower right panel, in both the e^+e^- and $\gamma\gamma$ processes. The vertical dashed gray lines indicate the current same-sign dilepton limits on the doubly-charged scalar mass from LHC [131,132], assuming a BR($H^{\pm\pm} \to \ell_\alpha^\pm \ell_\beta^\pm$) = 100%. See text for more details.

the production cross sections as functions of the coupling $f_{\alpha\beta}$ involved, and estimate the resultant prospects for the individual couplings at future lepton colliders like CEPC, ILC and FCC-ee. To be specific, we consider only the pair and single production at an ILC running of $\sqrt{s} = 1$ TeV in Fig. 28, as the planned CEPC and FCC-ee energies are lower. To be conservative, the ILC beams are assumed to be unpolarized; for the RH $H^{\pm\pm}$, polarized beams could improve to some extent the production cross sections and prospects, e.g., with $P_{e^-} = 0.8$ and $P_{e^+} = -0.3$ [65]. The basic cuts and efficiencies are the same as above, i.e., $p_T(\ell) = 10$ GeV, and $\epsilon_{e,\mu} \simeq 1$ and $\epsilon_\tau = 60\%$. The SM backgrounds for the pure lepton final states are well understood, with the τ decays causing some complications. In particular, the SM backgrounds with LFV like $(e^\pm\mu^\pm)(e^\mp\mu^\mp)$ are expected to be very low, and they might originate from e.g., particle misidentification [164,165]. With the well-controlled SM background, the on-shell $H^{\pm\pm}$ is expected to give rise to sharp resonancelike peaks over the continuous kinetic distributions of the charged leptons like the invariant mass $m(\ell^\pm\ell'^\pm)$ [47]. To be concrete, we assume a total number of 30 events for the signals without

apparent LFV like $H^{\pm\pm} \to e^\pm e^\pm$ and 10 for the LFV signals such as $H^{\pm\pm} \to e^\pm\mu^\pm$.

As already mentioned, only the electron and muon $g - 2$ and the LEP data could be used to set unambiguous limits on the Yukawa couplings $f_{\alpha\beta}$ for the Yukawa pair and single production modes. Suppressed by the small charged lepton masses in Eq. (39), the $g - 2$ limits in Table IV are very weak and are not shown in Fig. 28. For the few hundred GeV scale $H^{\pm\pm}$, the LEP $ee \to \ell\ell$ data exclude the couplings $f_{e\ell}$ of order $\mathcal{O}(0.1)$ with $\ell = e, \mu, \tau$, as presented in the first three plots of Fig. 28. The same-sign dilepton limits on the doubly-charged scalar mass from the ATLAS [131] and CMS [132] data in Fig. 21 are also shown in Fig. 28 as the vertical dashed gray lines, assuming a BR($H^{\pm\pm} \to \ell_\alpha^\pm \ell_\beta^\pm$) = 100% with respect to the specific lepton flavors $\ell_{\alpha,\beta}$. The dilepton limits for the states $\mu\tau$ and $\tau\tau$ are below 500 GeV and are not shown in the lower right panel of Fig. 28.

When $M_{\pm\pm} \lesssim \sqrt{s}/2 = 500$ GeV at ILC, the doubly-charged scalar can be either pair or single produced, via respectively the Yukawa couplings (the second diagram in Fig. 22) or the $e\gamma$ process (the middle row in Fig. 24). In the lighter mass range, the single-production-like processes
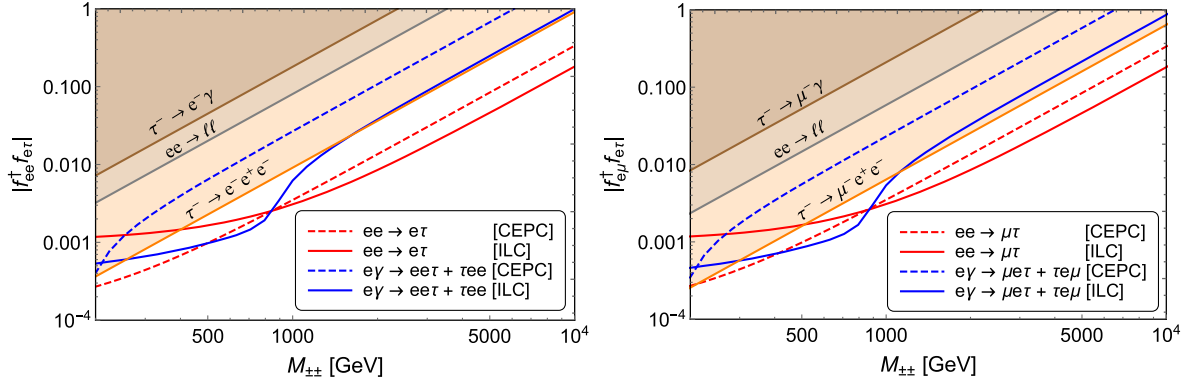
FIG. 29.   Prospects of the Yukawa couplings $|f^\dagger_{ee}f_{e\tau}|$ and $|f^\dagger_{e\mu}f_{e\tau}|$ for the doubly-charged scalar $H^{\pm\pm}$ production via the $ee \to \ell_\alpha\ell_\beta$ (red) and $e\gamma \to \ell_\alpha\ell_\beta\ell_\gamma$ (blue) processes, at CEPC with $\sqrt{s} = 240$ GeV and an integrated luminosity of 5 ab^{-1} (dashed) and at ILC with $\sqrt{s} = 1$ TeV and 1 ab^{-1} (solid). The shaded regions are excluded by the rare tauon decays $\tau \to \ell_\alpha\gamma$, $\tau \to \ell_\alpha\ell_\beta\ell_\gamma$ and the LEP $ee \to \ell\ell$ data [97]. See the text for more details.

e^+e^-, $\gamma\gamma \to H^{\pm\pm}\ell_\alpha^\mp\ell_\beta^\mp$ are in fact dominated by the pair-production modes e^+e^-, $\gamma\gamma \to H^{++}H^{--}$ in Fig. 22 which do not depend on the Yukawa couplings; thus all the ee and $\gamma\gamma$ single production processes in Fig. 28 are truncated at 500 GeV. As the pair-production amplitudes have a quadratic dependence on the couplings $f_{\alpha\beta}$ while the single $e\gamma$ process is only linear, the latter could probe a much smaller Yukawa coupling down to $\mathcal{O}(10^{-3})$ (the purple lines in the first three plots of Fig. 28), while the pair production only to a few times 10^{-2} (the orange lines).

For $M_{\pm\pm} \gtrsim \sqrt{s}/2$, only the single production modes ee (blue), $e\gamma$ (purple) and $\gamma\gamma$ (brown) are kinematically available. Compared to the $e\gamma$ processes, the ee and γ ones have one more lepton in the final state. Thus the cross sections are comparatively smaller (see Fig. 25), and the $\gamma\gamma$ modes are further suppressed by the effective photon luminosity function in Eq. (9). Though the $e\gamma$ cross sections are comparatively larger, they are limited to the couplings $f_{\alpha\beta}$ involving at least one electron; cf. the middle row diagrams in Fig. 24. The Yukawa couplings in the $\mu - \tau$ sector ($f_{\mu\mu}$, $f_{\mu\tau}$ and $f_{\tau\tau}$) could only be reached via the e^+e^- and $\gamma\gamma$ collisions, with the prospects collected in the lower right panel of Fig. 28. There is currently almost no limit on these couplings, except for the muon $g - 2$ on $f_{\mu\mu}$ and $f_{\mu\tau}$ which however is too weak to set any limits. Compared to the couplings involving at least one electron flavor, the production cross sections for those in the $\mu - \tau$ sector are much smaller, and the prospects are resultantly also much weaker, at most of order 10^{-2}. Nevertheless, all these modes are largely complementary to each other, in particular the ee and $e\gamma$ processes, in producing the doubly-charged scalars, revealing the flavor structure of the Yukawa couplings $f_{\alpha\beta}$ and hunting for the LFV signals.

For the off-shell production $e^+e^- \to \ell_\alpha\ell_\beta$ and $e\gamma \to \ell_\alpha\ell_\beta\ell_\gamma$, the doubly-charged scalar mass could be (much) higher than the center-of-mass energy of the lepton

colliders. For the sake of comparison we show in Figs. 29 and 30 the prospects at both CEPC with $\sqrt{s} = 240$ GeV and an integrated luminosity of 5 ab^{-1} and ILC with $\sqrt{s} = 1$ TeV and a luminosity of 1 ab^{-1}. With a higher luminosity at 240 GeV anticipated, the FCC-ee could do better than CEPC. As the production amplitudes depend quadratically on the couplings $f_{\alpha\beta}$, the experimental constraints on the Yukawa couplings $|f^\dagger f|$ are different from those for the on-shell production in Fig. 28, as clearly seen in Table IV. In particular, the limit from $\mu \to eee$ is so stringent that it leaves no probable space for $|f^\dagger_{ee}f_{e\mu}|$. The limits from the tauon sector are comparatively much weaker, with the prospects for $|f^\dagger_{ee}f_{e\tau}|$ and $|f^\dagger_{e\mu}f_{e\tau}|$ at CEPC and ILC via the $ee \to \ell_\alpha\ell_\beta$ and $e\gamma \to \ell_\alpha\ell_\beta\ell_\gamma$ processes collectively presented in Fig. 29. For $|f^\dagger_{ee}f_{e\tau}|$, the constraints are predominantly from the rare decays $\tau \to eee$ and $\tau \to e\gamma$, whereas the $\tau^- \to \mu^-e^+e^-$ and $\tau \to \mu\gamma$ data can be used to set limits on $|f^\dagger_{e\mu}f_{e\tau}|$. Given the limits on $|f_{e\ell}|$ (with $\ell = e, \mu, \tau$) from the $ee \to \ell\ell$ data at LEP [97], these combinations $|f^\dagger_{ee}f_{e\tau}|$ and $|f^\dagger_{e\mu}f_{e\tau}|$ are also constrained by the LEP data, as shown in Fig. 29.

With only two leptons in the final state, the cross sections for the $ee \to \ell_\alpha\ell_\beta$ processes are orders of magnitude larger than those for $e\gamma \to \ell_\alpha\ell_\beta\ell_\gamma$, as seen in Fig. 27; thus the former could probe smaller Yukawa couplings $|f^\dagger f|$, i.e., respectively $3.4 \times 10^{-9}(1.8 \times 10^{-9})$ GeV^{-2} at CEPC (ILC) for both $|f^\dagger_{ee}f_{e\tau}|$ and $|f^\dagger_{e\mu}f_{e\tau}|$ in the heavy doubly-charged scalar limit. These are well beyond the current limits from the rare three-body tauon decays, as seen in Fig. 29. Benefiting from the larger colliding energy, the ILC running at 1 TeV outperforms the CEPC. At ILC, when the doubly-charged scalar mass $M_{\pm\pm} \lesssim 1$ TeV, the $e\gamma$ process is actually dominated by the on-shell production $e\gamma \to \ell_\alpha H^{\pm\pm}$ with the subsequent decay $H^{\pm\pm} \to \ell_\beta^\pm\ell_\gamma^\pm$ (see the middle row in Fig. 25 for the Feynman diagrams),

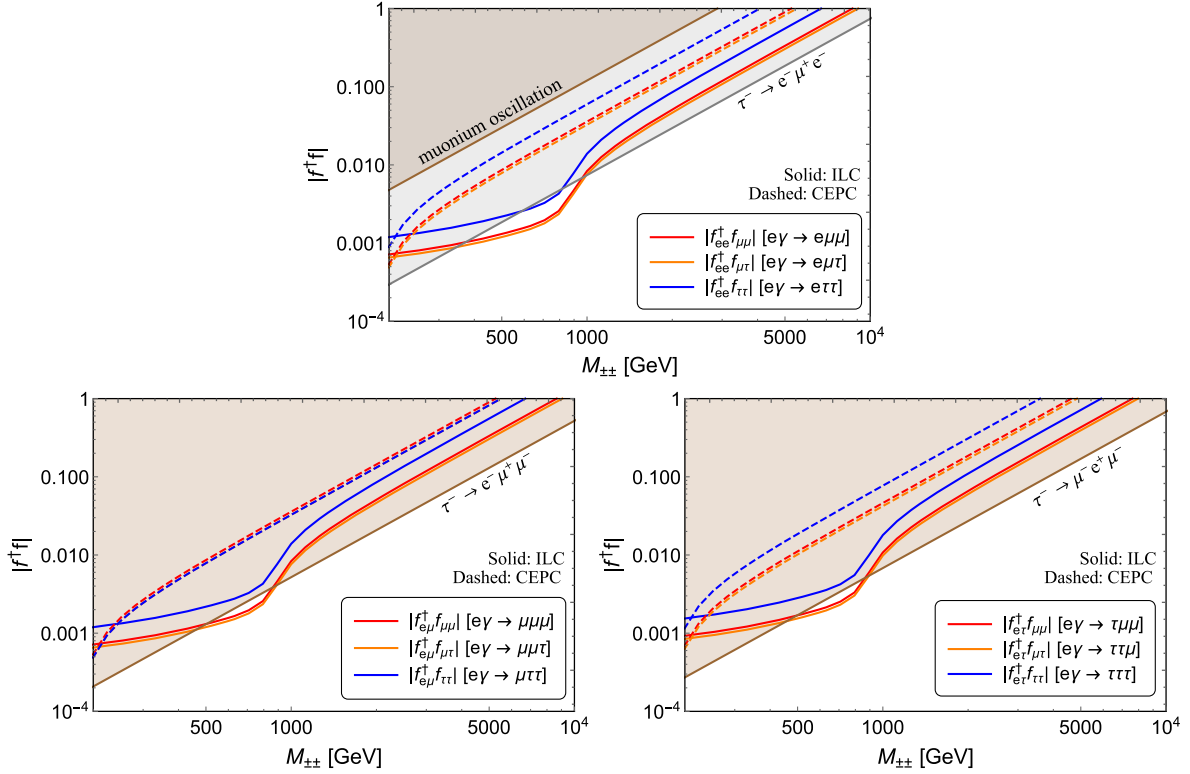FIG. 30.   The same as in Fig. 29, for the couplings $|f_{ee}^\dagger f_{\mu\mu}|$ (red), $|f_{ee}^\dagger f_{\mu\tau}|$ (orange) and $|f_{ee}^\dagger f_{\tau\tau}|$ (blue) in the upper panel; $|f_{e\mu}^\dagger f_{\mu\mu}|$ (red), $|f_{e\mu}^\dagger f_{\mu\tau}|$ (orange) and $|f_{e\mu}^\dagger f_{\tau\tau}|$ (blue) in the lower left panel; and $|f_{e\tau}^\dagger f_{\mu\mu}|$ (red), $|f_{e\tau}^\dagger f_{\mu\tau}|$ (orange) and $|f_{e\tau}^\dagger f_{\tau\tau}|$ (blue) in the lower right panel, at both CEPC (dashed) and ILC (solid). The shaded brown region is excluded by muonium oscillation, which is applicable to $|f_{ee}^\dagger f_{\mu\mu}|$ (cf. Table IV). The rare tauon decays $\tau^- \to e^- \mu^+ e^-$, $\tau^- \to e^- \mu^+ \mu^-$ and $\tau^- \to \mu^- e^+ \mu^-$ (gray) are used to constrain respectively the couplings $|f_{ee}^\dagger f_{\mu\tau}|$, $|f_{e\mu}^\dagger f_{\mu\tau}|$ and $|f_{e\tau}^\dagger f_{\mu\mu}|$ (cf. Table IV).

and the production cross sections in Fig. 27 and the prospects in Fig. 29 are largely enhanced, even better than the ee mode.

All other combinations of the lepton flavors in $f_{\alpha\beta}^\dagger f_{\gamma\delta}$ can be collected in the form of $f_{e\alpha}^\dagger f_{\beta\gamma}$ with $\alpha = e, \mu, \tau$ and $\beta, \gamma = \mu, \tau$. These couplings could only be probed via the processes $e^\pm \gamma \to \ell_\alpha^\mp \ell_\beta^\pm \ell_\gamma^\pm$, with the corresponding prospects at CEPC and ILC presented in the plots of Fig. 30. As in Fig. 29, when the doubly-charged scalar mass is below 1 TeV, it could be produced on shell at ILC and the prospects increase significantly. Given all the flavor constraints in Table IV, only some of the Yukawa couplings $|f^\dagger f|$ are constrained by current experimental data: muonium oscillation can be used to set a limit on $|f_{ee}^\dagger f_{\mu\mu}|$ (red curves in the upper panel), while the rare tauon decays $\tau^- \to e^- \mu^+ e^-$, $\tau^- \to e^- \mu^+ \mu^-$ and $\tau^- \to \mu^- e^+ \mu^-$ could be used to constrain respectively the couplings $|f_{ee}^\dagger f_{\mu\tau}|$ (orange curves in the upper panel), $|f_{e\mu}^\dagger f_{\mu\tau}|$ (orange curves in the lower left panel) and $|f_{e\tau}^\dagger f_{\mu\mu}|$ (red curves in the lower right panel). It is transparent in Fig. 30 that when these limits are taken into consideration, one would not see any signal at CEPC or ILC in these channels, unless the

doubly-charged scalar could be produced on shell. All the other combinations of couplings $|f^\dagger f|$ are not constrained by any data, and one could probe these couplings with the LFV signals by searching for the trileptons $e\gamma \to \ell_\alpha \ell_\beta \ell_\gamma$, even if the doubly-charged scalar mass is beyond the TeV scale.

D. Application to specific textures

In this section, we consider three specific textures of the matrix $f_{\alpha\beta}$ in Eq. (3) to exemplify the flavor constraints and lepton collider prospects of the RH doubly-charged scalar in the LRSM. Typically, the property of each case starts with specific textures of the charged lepton mass matrix, the Dirac neutrino mass matrix and the heavy RHN mass matrix in the LRSM, which give rise to the physical charged lepton masses, the tiny neutrino masses, the lepton flavor mixing angles and the CP violating phases [83]. With regard to the doubly-charged scalar sector, only the f coupling matrix is relevant, which is related to the heavy RHN masses via $M_N \simeq 2fv_R$. Three simple textures of f are presented in Table V, i.e., the textures A, B and C, which share the same sets of parameters, with only two free parameters $f_{1,2}$ of order $\mathcal{O}(0.1)$, following the numerical fit

TABLE V. Three specific sample textures A, B and C, for the coupling matrix f, with the fixed values of $f_{1,2}$ given in the table. We show collectively, for all three textures, the decay BRs, the flavor limits from Table IV (the lower bounds on M_{++} are put in the brackets with those lower than 100 GeV not shown), the LHC same-sign dilepton limits from Fig. 21 (the corresponding channels are in parentheses), the pair-production mass windows at ILC 1 TeV in the ee mode, the single production channels (the lepton pairs in parentheses are from on-shell $H^{\pm\pm}$ decay) in both the $ee/\gamma\gamma$ and $e\gamma$ modes, and the off-shell production channels of the ee and $e\gamma$ processes. For textures B and C, the on-shell production is not possible (as denoted by $-$), because of the stringent LHC limits. See the text for more details.

Textures	A	B	C
$f_1 = 0.1$ $f_2 = 0.5$	$\begin{pmatrix} 0 & f_1 & 0 \\ f_1 & 0 & 0 \\ 0 & 0 & f_2 \end{pmatrix}$	$\begin{pmatrix} f_2 & 0 & 0 \\ 0 & 0 & f_1 \\ 0 & f_1 & 0 \end{pmatrix}$	$\begin{pmatrix} 0 & 0 & f_1 \\ 0 & f_2 & 0 \\ f_1 & 0 & 0 \end{pmatrix}$
Decay BRs	$\mathrm{BR}(e\mu) = 7.4\%$ $\mathrm{BR}(\tau\tau) = 92.6\%$	$\mathrm{BR}(\mu\tau) = 7.4\%$ $\mathrm{BR}(ee) = 92.6\%$	$\mathrm{BR}(e\tau) = 7.4\%$ $\mathrm{BR}(\mu\mu) = 92.6\%$
Flavor limits	Electron $g-2$ Muon $g-2$ $ee \to \mu\mu$ (395 GeV)	$\tau^- \to e^-\mu^+ e^-$ (2.6 TeV) Electron $g-2$ Muon $g-2$ $ee \to ee$ (1.4 TeV)	$\tau^- \to \mu^- e^+\mu^-$ (1.7 TeV) Electron $g-2$ Muon $g-2$ $ee \to \tau\tau$ (430 GeV)
LHC limits	321 GeV ($e\mu$)	648 GeV (ee)	710 GeV ($\mu\mu$)
Pair production at ILC 1 TeV	[395, 500] GeV	$\cdots$	$\cdots$
Single production ($ee, \gamma\gamma$)	$(e^\pm\mu^\pm)e^\mp\mu^\mp$ $(e^\pm\mu^\pm)\tau^\mp\tau^\mp$ $(\tau^\pm\tau^\pm)e^\mp\mu^\mp$ $(\tau^\pm\tau^\pm)\tau^\mp\tau^\mp$	$\cdots$	$\cdots$
Single production ($e\gamma$)	$(e^\pm\mu^\pm)\mu^\mp$ $(\tau^\pm\tau^\pm)\mu^\mp$	$\cdots$	$\cdots$
Off-shell production (ee)	$\mu^+\mu^-$	e^+e^-	$\tau^+\tau^-$
Off-shell production ($e\gamma$)	$\mu^\mp e^\pm\mu^\pm$ $\mu^\mp\tau^\pm\tau^\pm$	$e^\mp e^\pm e^\pm$ $e^\mp\mu^\pm\tau^\pm$	$\tau^\mp e^\pm\tau^\pm$ $\tau^\mp\mu^\pm\mu^\pm$

of Ref. [83]. The texture zeros might originate from and be protected by some underlying discrete symmetry groups in the lepton sector [78,83].

For the texture A, the doubly-charged scalar decays predominantly into $e^\pm\mu^\pm$ and $\tau^\pm\tau^\pm$; following Eq. (36), the BR are respectively 7.4% and 92.6%, as collected in Table V. With the texture zeros, some of the flavor constraints in Table IV are not applicable to this specific scenario; only the electron and muon $g-2$ and the LEP $ee \to \mu\mu$ data set limits on the $f_{1,2}$ couplings, depending on the doubly-charged scalar mass M_{++}. Among them, the most stringent is from the LEP data, which requires that $M_{++} > 395$ GeV (cf. the upper right panel of Fig. 28), and the $g-2$ limits are below 100 GeV. Regarding the ATLAS and CMS same-sign dilepton limits in Fig. 21, it is trivial to interpret the $e\mu$ and $\tau\tau$ data with respect to the corresponding BRs and to obtain the constraints on a doubly-charged scalar mass, which turn out to be 321 GeV ($e\mu$) and 253 GeV ($\tau\tau$).

Combining all the limits above, there is only a narrow window left for the pair production of $H^{\pm\pm}$ at the ILC running at 1 TeV: 395 GeV $< M_{++} <$ 500 GeV, with

nevertheless a strikingly clear signal in particular in the $e\mu$ channel[15]:

$$e^+e^- \to \gamma^*/Z^* \to H^{++}H^{--}$$
$$\to (e^+\mu^+)(e^-\mu^-), (e^\pm\mu^\pm)(\tau^\mp\tau^\mp), (\tau^+\tau^+)(\tau^-\tau^-).$$
(47)

With the $\mathcal{O}(0.1)$ Yukawa couplings $f_{1,2}$, the doubly-charged scalar is hard to miss at lepton colliders by reconstructing the invariant mass $m_{e\mu}$ and $m_{\tau\tau}$ of the same-sign dilepton pairs. One should note that the doubly-charged scalar could also be produced through the Yukawa coupling $f_{e\mu}$ (cf. the second diagram in Fig. 22), which is however comparatively suppressed by a factor of $(f_1/e)^4$ (e here being the electric charge) and thus contributes only with a factor of $\sim[1 + (f_{e\mu}/e)^2]$ to the total cross section for the pair production of $H^{\pm\pm}$.

---

[15]For a doubly-charged scalar with mass $M_{++} > 395$ GeV, the production $\gamma\gamma \to H^{++}H^{--}$ is only marginally allowed at ILC 1 TeV, as seen in Fig. 23.

When the doubly-charged scalar is heavier than 500 GeV, it could only be single produced at ILC from the ee, $\gamma\gamma$ and $e\gamma$ processes, with potentially all the flavor combinations listed in the first column of Table V. Roughly speaking, with the initial ee or $\gamma\gamma$, the doubly-charged scalar can be produced in association with the same-sign lepton pairs of $e^\pm\mu^\pm$ or $\tau^\pm\tau^\pm$, while for the $e\gamma$ process, the doubly-charged scalar can be produced with a muon, which is dictated by the f_1 coupling. If the doubly-charged scalar is too heavy to be directly produced on shell, it could yet mediate the processes $e^+e^- \to \mu^+\mu^-$ and $e^\pm\gamma \to \mu^\mp e^\pm\mu^\pm, \mu^\mp\tau^\pm\tau^\pm$. The doubly-charged scalar mediated $ee \to \mu\mu$ would interfere with the SM background, altering both the total cross section and angular distributions, thus constrained by the LEP data [97]. The doubly-charged scalar mediated $\mu^\mp e^\pm\mu^\pm$ process will also interfere with the pure SM diagrams of $e^\pm\gamma \to e^\pm\mu^\pm\mu^\mp$ and might have effects on both the cross section and differential distributions, depending on the mass $M_{\pm\pm}$. A dedicated analysis is beyond the main scope of this paper and we will not go into any further details. The $\mu^\mp\tau^\pm\tau^\pm$ final states are, on the contrary, clear signatures of LFV, even if the doubly-charged scalar goes beyond the TeV scale.

By replacing $1 \leftrightarrow 3$ and $2 \leftrightarrow 3$ in the matrix f of texture A, we obtain respectively scenarios B and C. With the textures changed, the lepton flavor constraints also vary, which are all collected in the second and third column of Table V. For scenario B, the most stringent limits are from the rare decay $\tau^- \to e^-\mu^+e^-$ which requires that $M_{\pm\pm} >$ 2.6 TeV for the specific values of $f_{1,2}$ (cf. the upper panel of Fig. 30). The electron and muon $g-2$ limits are below 100 GeV and are not shown in the table. The coupling $f_{ee} = f_2$ induces also extra contribution to the Bhabha scattering and is thus tightly constrained by the LEP data with a lower bound of 1.4 TeV on the doubly-charged scalar mass. With these overwhelming limits, the $H^{\pm\pm}$ can only be produced at ILC 1 TeV in the off-shell mode, producing the LFV signal of $e^\pm\gamma \to e^\mp\mu^\pm\tau^\pm$, though the on-shell production is possible at CLIC 3 TeV.[16] In addition, the large branching fraction into ee pushes the LHC dilepton limits on $M_{\pm\pm}$ much more stringently than texture A, being 648 GeV.

Texture C is kind of similar to texture B, with the doubly-charged scalar decaying predominantly into $\mu^\pm\mu^\pm$ with a small proportion to $e^\pm\tau^\pm$. The rare decay $\tau^- \to \mu^-e^+\mu^-$ provides the most stringent flavor constraints of 1.7 TeV on the doubly-charged scalar mass (cf. the lower right panel of Fig. 30). The limit from the LEP $ee \to \tau\tau$ data is comparatively much weaker, roughly 430 GeV, suppressed to some extent by the coupling f_1. The LHC same-sign dilepton limit is somewhat stronger than in scenario B and is 710 GeV. With a beyond-TeV scale $H^{\pm\pm}$, the LFV

signal in the off-shell mode is primarily $\tau^\mp\mu^\pm\mu^\pm$, in addition to the lepton-flavor-conserving-like process $e^\pm\tau^\pm\tau^\mp$, from the $e\gamma$ collision.

Although the three textures A, B and C share the same data set of $f_{1,2}$, their implications on the searches of $H^{\pm\pm}$ at future lepton colliders are distinctly different, e.g., the flavor limits on the doubly-charged scalar mass and the on-shell and off-shell signals. Given the prospects in Sec. IV B, these realistic models could easily be tested and distinguished at future lepton colliders, e.g., via searches of the LFV signals and direct (pair) production of doubly-charged scalars. In the LRSM with a multi-TeV scale RH scale v_R, say 5 TeV, to accommodate TeV scale RHNs for the seesaw mechanism, (some of) the f elements are expected to be sizable. In the absence of any beyond-SM signal at lepton colliders, these scenarios will be clearly ruled out. More importantly, it might imply that the RH scale v_R is much heavier than the TeV scale and hence the W_R mass will be pushed beyond the LHC capability by the absence of these signals, which will anyway be an interesting result in the study of TeV scale left-right seesaw models for neutrino masses.

V. CONCLUSION

In this paper we have studied in great detail the prospects for observing the effects of triplet scalars of the left-right symmetric model in future lepton colliders, i.e., the neutral $SU(2)_R$-breaking scalar H_3 and its doubly-charged scalar partner $H^{\pm\pm}$. In the original Lagrangian, the neutral scalar H_3 couples only to the heavy beyond-SM scalar, the heavy W_R and Z_R gauge boson, and the heavy right-handed neutrinos, and not to any SM quarks. Thus it could easily evade all the current direct searches at the LHC. Via its mixing in the scalar sector and the neutrino sector, it could be produced in lepton colliders from fusion of the doubly-charged scalars, the radiative couplings to photons at the one-loop level, the mixing with the SM Higgs, the Yukawa couplings to the heavy neutrinos, and the mixing with the heavy neutral scalar H_1 from the bidoublet. From the phenomenological point of view, the most interesting channel is the last one, as the mixing with H_1 would lead to the LFV couplings of H_3, which is directly connected to the Dirac mass matrix in the seesaw formula. Given these LFV couplings, the neutral scalar H_3 can be produced in future lepton colliders on shell or off shell, leading to strikingly clear LFV signals such as $e^+e^- \to e^\pm\mu^\mp + H_3$ and $e^+e^- \to \mu^\pm\tau^\pm$. The Feynman diagrams can be found in Figs. 9, 11, 13 and 15, with the cross sections depicted in Figs. 10, 12, 14 and 16. With an integrated luminosity of the order of ab^{-1}, the couplings can be probed up to $\sim 10^{-4}$ (see Figs. 18 and 19), depending on the center-of-mass energy, the production channel and decay products. This is well beyond the current stringent flavor constraints in the lepton sector (see Table II) such as $\tau \to eee$ and $\mu \to e\gamma$ in a larger parameter space, and it could explain the muon $g-2$ anomaly in the channel $ee \to \mu\tau + H_3$.

---

[16]This is currently under investigation for an upcoming Yellow report on CLIC physics potential.

Regarding the right-handed doubly-charged scalar in the left-right symmetric model, its couplings to the charged leptons stem from type-II seesaw and point directly to the masses and flavor structure in the right-handed neutrino sector. We provide a full list of the production of doubly-charged scalars at future lepton colliders, through the e^+e^-, $e\gamma$ and $\gamma\gamma$ collisions (γ here refers to the real laser photon), in the channels of pair production, single production (in association with one or two additional charged leptons in the final state) and off-shell production, and with all the possible charge lepton flavor combinations. The representative Feynman diagrams can be found in Figs. 22, 24 and 26, and the production cross sections are collected in Figs. 23, 25 and 27. The prospects are presented in Figs. 28–30. The lepton flavor conserving and violating coupling can be probed up to $\sim 10^{-3}$ for a large range of doubly-charged scalar masses that are well beyond the current flavor constraints listed in Table IV. As exemplified in Table V, the flavor limits and lepton collider prospects depend largely on the structure of the Yukawa coupling f.

The neutral and doubly-charged seesaw scalars are intimately correlated to the tiny neutrino mass generation via the seesaw mechanism. The lepton collider searches of these scalars are largely complementary to the effects at current and future hadron colliders and the low-energy neutrino experiments such as those aiming at the leptonic CP violation, neutrino mass hierarchy and neutrinoless double beta decays. Due to the "clean" background of lepton colliders, the direct searches of the neutral and doubly-charged scalar at CEPC, ILC, FCC-ee and CLIC are very promising, and they might reveal the beyond-SM physics in searches of the LFV signals. These searches can even be connected to the dark matter particle in the type-II seesaw frameworks in a different class of left-right models with the lightest right-handed neutrino being the dark matter [166–168].

[1] F. del Aguila, E. Laermann, and P. M. Zerwas, Nucl. Phys. **B297,** 1 (1988).

[2] M. Dittmar, A. Santamaria, M. C. Gonzalez-Garcia, and J. W. F. Valle, Nucl. Phys. **B332,** 1 (1990).

[3] W. Buchmuller and C. Greub, Nucl. Phys. **B363,** 345 (1991).

[4] A. Djouadi, Z. Phys. C **63,** 317 (1994).

[5] G. Azuelos and A. Djouadi, Z. Phys. C **63,** 327 (1994).

[6] J. Gluza and M. Zralek, Phys. Lett. B **362,** 148 (1995).

[7] G. Belanger, F. Boudjema, D. London, and H. Nadeau, Phys. Rev. D **53,** 6292 (1996).

[8] J. Gluza and M. Zralek, Phys. Lett. B **372,** 259 (1996).

[9] B. Ananthanarayan and P. Minkowski, Phys. Lett. B **373,** 130 (1996).

[10] J. Gluza and M. Zralek, Phys. Rev. D **55,** 7030 (1997).

[11] J. Gluza, J. Maalampi, M. Raidal, and M. Zralek, Phys. Lett. B **407,** 45 (1997).

[12] P. Abreu et al. (DELPHI Collaboration), Z. Phys. C **74,** 57 (1997); **75,** 580(E) (1997).

[13] M. Raidal, Phys. Lett. B **492,** 107 (2000).

[14] W. Porod, M. Hirsch, J. Romao, and J. W. F. Valle, Phys. Rev. D **63,** 115004 (2001).

[15] P. Achard et al. (L3 Collaboration), Phys. Lett. B **517,** 67 (2001).

[16] D. Aristizabal Sierra, M. Hirsch, J. W. F. Valle, and A. Villanova del Moral, Phys. Rev. D **68,** 033006 (2003).

[17] F. Deppisch, H. Pas, A. Redelbach, R. Ruckl, and Y. Shimizu, Phys. Rev. D **69,** 054014 (2004).

[18] O. Cakir, I. Turk Cakir, and Z. Kirca, Phys. Rev. D **70,** 075017 (2004).

[19] F. del Aguila, J. A. Aguilar-Saavedra, A. Martinez de la Ossa, and D. Meloni, Phys. Lett. B **613,** 170 (2005).

[20] F. del Aguila and J. A. Aguilar-Saavedra, J. High Energy Phys. 05 (2005) 026.

[21] A. K. Ciftci, R. Ciftci, and S. Sultansoy, Phys. Rev. D **72,** 053006 (2005).

[22] S. Bray, J. S. Lee, and A. Pilaftsis, Phys. Lett. B **628,** 250 (2005).

[23] D. Atwood, S. Bar-Shalom, and A. Soni, Phys. Rev. D **76,** 033004 (2007).

[24] Y. B. Liu, Y. H. Cao, and H. M. Han, Eur. Phys. J. C **53,** 615 (2008).

[25] M. Kadastik, M. Raidal, and L. Rebane, Phys. Rev. D **77,** 115023 (2008).

[26] J. McDonald, N. Sahu, and U. Sarkar, J. Cosmol. Astropart. Phys. 04 (2008) 037.

[27] D. Aristizabal Sierra, J. Kubo, D. Restrepo, D. Suematsu, and O. Zapata, Phys. Rev. D **79,** 013011 (2009).

[28] A. Arhrib, B. Bajc, D. K. Ghosh, T. Han, G. Y. Huang, I. Puljak, and G. Senjanovic, Phys. Rev. D **82,** 053004 (2010).

[29] C. X. Yue, H. L. Feng, and W. Ma, Chin. Phys. Lett. **27,** 011202 (2010).

[30] W. Rodejohann, Phys. Rev. D **81,** 114001 (2010).

[31] J. Barry, L. Dorame, and W. Rodejohann, Eur. Phys. J. C **72,** 2023 (2012).

[32] A. Das and N. Okada, Phys. Rev. D **88,** 113001 (2013).

[33] B. Vormwald and J. List, Eur. Phys. J. C **74,** 2720 (2014).

[34] F. F. Freitas, C. A. de S. Pires, and P. S. Rodrigues da Silva, Phys. Lett. B **769,** 48 (2017).

[35] A. Blondel *et al.* (FCC-ee Study Team), Nucl. Part. Phys. Proc. **273**–**275**, 1883 (2016).
[36] S. Antusch and O. Fischer, J. High Energy Phys. 05 (2015) 053.
[37] S. Banerjee, P. S. B. Dev, A. Ibarra, T. Mandal, and M. Mitra, Phys. Rev. D **92**, 075002 (2015).
[38] T. Asaka and T. Tsuyuki, Phys. Rev. D **92**, 094012 (2015).
[39] S. Antusch, E. Cazzato, and O. Fischer, J. High Energy Phys. 04 (2016) 189.
[40] S. Antusch, E. Cazzato, and O. Fischer, J. High Energy Phys. 12 (2016) 007.
[41] K. Wang, T. Xu, and L. Zhang, Phys. Rev. D **95**, 075021 (2017).
[42] S. Antusch, E. Cazzato, and O. Fischer, Int. J. Mod. Phys. A **32**, 1750078 (2017).
[43] S. S. Biswal and P. S. B. Dev, Phys. Rev. D **95**, 115031 (2017).
[44] M. Chekkal, A. Ahriche, A. B. Hammou, and S. Nasri, Phys. Rev. D **95**, 095025 (2017).
[45] C. X. Yue, Y. C. Guo, and Z. H. Zhao, Nucl. Phys. **B925**, 186 (2017).
[46] W. Liao and X. H. Wu, Phys. Rev. D **97**, 055005 (2018).
[47] P. S. B. Dev, R. N. Mohapatra, and Y. Zhang, Phys. Rev. Lett. **120**, 221804 (2018).
[48] Y. Sui and Y. Zhang, Phys. Rev. D **97**, 095002 (2018).
[49] P. Agrawal, M. Mitra, S. Niyogi, S. Shil, and M. Spannowsky, Phys. Rev. D **98**, 015024 (2018).
[50] G. C. Cho, Y. Fukuda, and T. Kono, arXiv:1803.10475.
[51] F. F. Deppisch, P. S. B. Dev, and A. Pilaftsis, New J. Phys. **17**, 075019 (2015).
[52] Y. Cai, T. Han, T. Li, and R. Ruiz, Front. Phys. **6**, 40 (2018).
[53] P. Minkowski, Phys. Lett. **67B**, 421 (1977).
[54] R. N. Mohapatra and G. Senjanović, Phys. Rev. Lett. **44**, 912 (1980).
[55] T. Yanagida, Conf. Proc. C **7902131**, 95 (1979).
[56] M. Gell-Mann, P. Ramond, and R. Slansky, Conf. Proc. C **790927**, 315 (1979).
[57] S. L. Glashow, NATO Sci. Ser. B **61**, 687 (1980).
[58] J. C. Pati and A. Salam, Phys. Rev. D **10**, 275 (1974); **11**, 703(E) (1975).
[59] R. N. Mohapatra and J. C. Pati, Phys. Rev. D **11**, 2558 (1975).
[60] G. Senjanovic and R. N. Mohapatra, Phys. Rev. D **12**, 1502 (1975).
[61] P. S. B. Dev, R. N. Mohapatra, and Y. Zhang, J. High Energy Phys. 05 (2016) 174.
[62] P. S. B. Dev, R. N. Mohapatra, and Y. Zhang, Phys. Rev. D **95**, 115001 (2017).
[63] P. S. B. Dev, R. N. Mohapatra, and Y. Zhang, Nucl. Phys. **B923**, 179 (2017).
[64] CEPC-SPPC Study Group, Reports No. IHEP-CEPC-DR-2015-01, No. IHEP-TH-2015-01, No. IHEP-EP-2015-01, http://cepc.ihep.ac.cn/preCDR/main_preCDR.pdf.
[65] H. Baer *et al.*, arXiv:1306.6352.
[66] M. Bicer *et al.* (TLEP Design Study Working Group), J. High Energy Phys. 01 (2014) 164.
[67] E. Accomando *et al.* (CLIC Physics Working Group), arXiv:hep-ph/0412251.
[68] W. Y. Keung and G. Senjanovic, Phys. Rev. Lett. **50**, 1427 (1983).

[69] A. Ferrari, J. Collot, M. L. Andrieux, B. Belhorma, P. de Saintignon, J. Y. Hostachy, P. Martin, and M. Wielers, Phys. Rev. D **62**, 013001 (2000).
[70] M. Nemevsek, F. Nesti, G. Senjanovic, and Y. Zhang, Phys. Rev. D **83**, 115014 (2011).
[71] S. P. Das, F. F. Deppisch, O. Kittel, and J. W. F. Valle, Phys. Rev. D **86**, 055006 (2012).
[72] C. Y. Chen, P. S. B. Dev, and R. N. Mohapatra, Phys. Rev. D **88**, 033014 (2013).
[73] P. S. B. Dev, D. Kim, and R. N. Mohapatra, J. High Energy Phys. 01 (2016) 118.
[74] M. Mitra, R. Ruiz, D. J. Scott, and M. Spannowsky, Phys. Rev. D **94**, 095016 (2016).
[75] M. Nemevek, F. Nesti, and G. Popara, Phys. Rev. D **97**, 115018 (2018).
[76] M. Tanabashi *et al.* (Particle Data Group), Phys. Rev. D **98**, 030001 (2018).
[77] J. Gluza, Acta Phys. Pol. B **33**, 1735 (2002).
[78] J. Kersten and A. Y. Smirnov, Phys. Rev. D **76**, 073005 (2007).
[79] Z. z. Xing, Prog. Theor. Phys. Suppl. **180**, 112 (2009).
[80] X. G. He, S. Oh, J. Tandean, and C. C. Wen, Phys. Rev. D **80**, 073012 (2009).
[81] R. Adhikari and A. Raychaudhuri, Phys. Rev. D **84**, 033002 (2011).
[82] A. Ibarra, E. Molinaro, and S. T. Petcov, J. High Energy Phys. 09 (2010) 108.
[83] C. H. Lee, P. S. B. Dev, and R. N. Mohapatra, Phys. Rev. D **88**, 093010 (2013).
[84] M. Mitra, G. Senjanovic, and F. Vissani, Nucl. Phys. **B856**, 26 (2012).
[85] J. A. Aguilar-Saavedra and F. R. Joaquim, Phys. Rev. D **86**, 073005 (2012).
[86] P. S. B. Dev, R. N. Mohapatra, and Y. Zhang, J. High Energy Phys. 03 (2018) 122.
[87] J. A. Grifols, A. Mendez, and G. A. Schuler, Mod. Phys. Lett. A **04**, 1485 (1989).
[88] Y. Zhang, H. An, X. Ji, and R. N. Mohapatra, Nucl. Phys. **B802**, 247 (2008).
[89] A. Maiezza, G. Senjanovi, and J. C. Vasquez, Phys. Rev. D **95**, 095004 (2017).
[90] S. R. Coleman and E. J. Weinberg, Phys. Rev. D **7**, 1888 (1973).
[91] A. Maiezza, M. Nemevsek, F. Nesti, and G. Senjanovic, Phys. Rev. D **82**, 055022 (2010).
[92] G. Senjanović and V. Tello, Phys. Rev. Lett. **119**, 201803 (2017).
[93] M. Nemevšek, F. Nesti, and J. C. Vasquez, J. High Energy Phys. 04 (2017) 114.
[94] M. Nemevšek, G. Senjanovic, and V. Tello, Phys. Rev. Lett. **110**, 151802 (2013).
[95] X. Lou, ICHEP2018, Seoul.
[96] A. Belyaev, N. D. Christensen, and A. Pukhov, Comput. Phys. Commun. **184**, 1729 (2013).
[97] J. Abdallah *et al.* (DELPHI Collaboration), Eur. Phys. J. C **45**, 589 (2006).
[98] I. F. Ginzburg, G. L. Kotkin, V. G. Serbo, and V. I. Telnov, Nucl. Instrum. Methods Phys. Res. **205**, 47 (1983).

[99] I. F. Ginzburg, G. L. Kotkin, S. L. Panfil, V. G. Serbo, and V. I. Telnov, Nucl. Instrum. Methods Phys. Res., Sect. A **219**, 5 (1984).

[100] V. I. Telnov, Nucl. Instrum. Methods Phys. Res., Sect. A **294**, 72 (1990).

[101] A. Falkowski, C. Gross, and O. Lebedev, J. High Energy Phys. 05 (2015) 057.

[102] J. C. Helo, M. Hirsch, and S. Kovalenko, Phys. Rev. D **89**, 073005 (2014); **93**, 099902(E) (2016).

[103] G. Cottin, J. C. Helo, and M. Hirsch, Phys. Rev. D **97**, 055025 (2018).

[104] R. Barate *et al.* (ALEPH, DELPHI, L3, OPAL Collaborations and LEP Working Group for Higgs Boson Searches), Phys. Lett. B **565**, 61 (2003).

[105] ATLAS Collaboration, Report No. ATLAS-CONF-2016-073.

[106] S. Chatrchyan *et al.* (CMS Collaboration), Phys. Rev. D **89**, 092007 (2014).

[107] V. Khachatryan *et al.* (CMS Collaboration), J. High Energy Phys. 10 (2015) 144.

[108] G. Aad *et al.* (ATLAS Collaboration), Eur. Phys. J. C **76**, 45 (2016).

[109] M. Aaboud *et al.* (ATLAS Collaboration), J. High Energy Phys. 09 (2016) 173.

[110] G. Aad *et al.* (ATLAS Collaboration), Phys. Rev. Lett. **113**, 171801 (2014).

[111] ATLAS Collaboration, Report No. ATLAS-CONF-2016-059.

[112] V. Khachatryan *et al.* (CMS Collaboration), Phys. Lett. B **767**, 147 (2017).

[113] V. Khachatryan *et al.* (CMS Collaboration), Phys. Lett. B **749**, 560 (2015).

[114] ATLAS Collaboration, Report No. ATLAS-CONF-2016-049.

[115] V. Khachatryan *et al.* (CMS Collaboration), Phys. Rev. D **94**, 052012 (2016).

[116] Y. Amhis *et al.* (HFLAV Collaboration), Eur. Phys. J. C **77**, 895 (2017).

[117] D. Hanneke, S. Fogwell, and G. Gabrielse, Phys. Rev. Lett. **100**, 120801 (2008).

[118] G. W. Bennett *et al.* (Muon g-2 Collaboration), Phys. Rev. D **73**, 072003 (2006).

[119] L. Willmann *et al.*, Phys. Rev. Lett. **82**, 49 (1999).

[120] M. Sher and Y. Yuan, Phys. Rev. D **44**, 1461 (1991).

[121] R. Harnik, J. Kopp, and J. Zupan, J. High Energy Phys. 03 (2013) 026.

[122] G. Blankenburg, J. Ellis, and G. Isidori, Phys. Lett. B **712**, 386 (2012).

[123] M. Lindner, M. Platscher, and F. S. Queiroz, Phys. Rep. **731**, 1 (2018).

[124] T. E. Clark and S. T. Love, Mod. Phys. Lett. A **19**, 297 (2004).

[125] U. D. Jentschura, G. Soff, V. G. Ivanov, and S. G. Karshenboim, Phys. Rev. A **56**, 4483 (1997).

[126] U. D. Jentschura, S. G. Karshenboim, V. G. Ivanov, and G. Soff, Phys. Lett. B **424**, 397 (1998).

[127] I. F. Ginzburg, U. D. Jentschura, S. G. Karshenboim, F. Krauss, V. G. Serbo, and G. Soff, Phys. Rev. C **58**, 3565 (1998).

[128] W. S. Hou and G. G. Wong, Phys. Rev. D **53**, 1537 (1996).

[129] V. V. Kabachenko and Y. F. Pirogov, Eur. Phys. J. C **4**, 525 (1998).

[130] G. C. Cho and H. Shimo, Mod. Phys. Lett. A **32**, 1750127 (2017).

[131] ATLAS Collaboration, Report No. ATLAS-CONF-2017-053.

[132] CMS Collaboration, Report No. CMS-PAS-HIG-16-036.

[133] D. Chang, R. N. Mohapatra, and M. K. Parida, Phys. Rev. Lett. **52**, 1072 (1984).

[134] M. Magg and C. Wetterich, Phys. Lett. **94B**, 61 (1980).

[135] J. Schechter and J. W. F. Valle, Phys. Rev. D **22**, 2227 (1980).

[136] T. P. Cheng and L.-F. Li, Phys. Rev. D **22**, 2860 (1980).

[137] G. Lazarides, Q. Shafi, and C. Wetterich, Nucl. Phys. **B181**, 287 (1981).

[138] R. N. Mohapatra and G. Senjanovic, Phys. Rev. D **23**, 165 (1981).

[139] S. Bertolini, A. Maiezza, and F. Nesti, Phys. Rev. D **89**, 095028 (2014).

[140] A. Djouadi, Phys. Rep. **457**, 1 (2008).

[141] A. G. Akeroyd, M. Aoki, and H. Sugiyama, Phys. Rev. D **79**, 113010 (2009).

[142] D. N. Dinh, A. Ibarra, E. Molinaro, and S. T. Petcov, J. High Energy Phys. 08 (2012) 125; 09 (2013) 23.

[143] R. N. Mohapatra, Phys. Rev. D **46**, 2990 (1992).

[144] J. P. Leveille, Nucl. Phys. **B137**, 63 (1978).

[145] S. R. Moore, K. Whisnant, and B. L. Young, Phys. Rev. D **31**, 105 (1985).

[146] J. F. Gunion, J. Grifols, A. Mendez, B. Kayser, and F. I. Olness, Phys. Rev. D **40**, 1546 (1989).

[147] P. Herczeg and R. N. Mohapatra, Phys. Rev. Lett. **69**, 2475 (1992).

[148] M. L. Swartz, Phys. Rev. D **40**, 1521 (1989).

[149] G. Abbiendi *et al.* (OPAL Collaboration), Phys. Lett. B **577**, 93 (2003).

[150] P. Achard *et al.* (L3 Collaboration), Phys. Lett. B **576**, 18 (2003).

[151] J. Benesch *et al.* (MOLLER Collaboration), arXiv:1411.4088.

[152] P. S. B. Dev, M. J. Ramsey-Musolf, and Y. Zhang, Phys. Rev. D **98**, 055013 (2018).

[153] M. Kuze and Y. Sirois, Prog. Part. Nucl. Phys. **50**, 1 (2003); **53**, 679 (2004).

[154] S. Chakrabarti, D. Choudhury, R. M. Godbole, and B. Mukhopadhyaya, Phys. Lett. B **434**, 347 (1998).

[155] G. Tavares-Velasco and J. J. Toscano, Phys. Lett. B **472**, 105 (2000).

[156] G. Barenboim, K. Huitu, J. Maalampi, and M. Raidal, Phys. Lett. B **394**, 132 (1997).

[157] M. Lusignoli and S. Petrarca, Phys. Lett. B **226**, 397 (1989).

[158] C. X. Yue and S. Zhao, Eur. Phys. J. C **50**, 897 (2007).

[159] S. Godfrey, P. Kalyniak, and N. Romanenko, Phys. Rev. D **65**, 033009 (2002).

[160] S. Godfrey, P. Kalyniak, and N. Romanenko, Phys. Lett. B **545**, 361 (2002).

[161] T. G. Rizzo, Phys. Rev. D **25**, 1355 (1982); **27**, 657(A) (1983).

[162] C. X. Yue, S. Zhao, and W. Ma, Nucl. Phys. **B784**, 36 (2007).

[163] P. S. Bhupal Dev and Y. Zhang, arXiv:1808.00943.

[164] C. Milstene, G. Fisk, and A. Para, J. Instrum. **1**, P10003 (2006).

[165] D. Yu, M. Ruan, V. Boudry, and H. Videau, Eur. Phys. J. C **77**, 591 (2017).

[166] P. S. B. Dev, D. Kazanas, R. N. Mohapatra, V. L. Teplitz, and Y. Zhang, J. Cosmol. Astropart. Phys. 08 (2016) 034.

[167] P. S. B. Dev, R. N. Mohapatra, and Y. Zhang, J. High Energy Phys. 11 (2016) 077.

[168] P. S. B. Dev, R. N. Mohapatra, and Y. Zhang, Mod. Phys. Lett. A **32**, 1740007 (2017).